PERFORMANCE OF CYCLOIDAL PROPELLERS IN CAVITATING ENVIRONMENT

G. F. Dobay, et al

David W. Taylor Naval Ship Research
and Development Center
Bethesda, Maryland

December 1969

DAVID W. TAYLOR
NAVAL SHIP RESEARCH AND DEVELOPMENT CENTER
Bethesda, Maryland 20084

PERFORMANCE OF CYCLOIDAL PROPELLERS IN CAVITATING ENVIRONMENT

by

G. F. Dobay and M. C. Dickerson

APPROVED FOR PUBLIC RELEASE: DISTRIBUTION UNLIMITED

SHIP PERFORMANCE DEPARTMENT

December 1969

SPD-363-01

MAJOR DTNSRDC ORGANIZATIONAL COMPONENTS

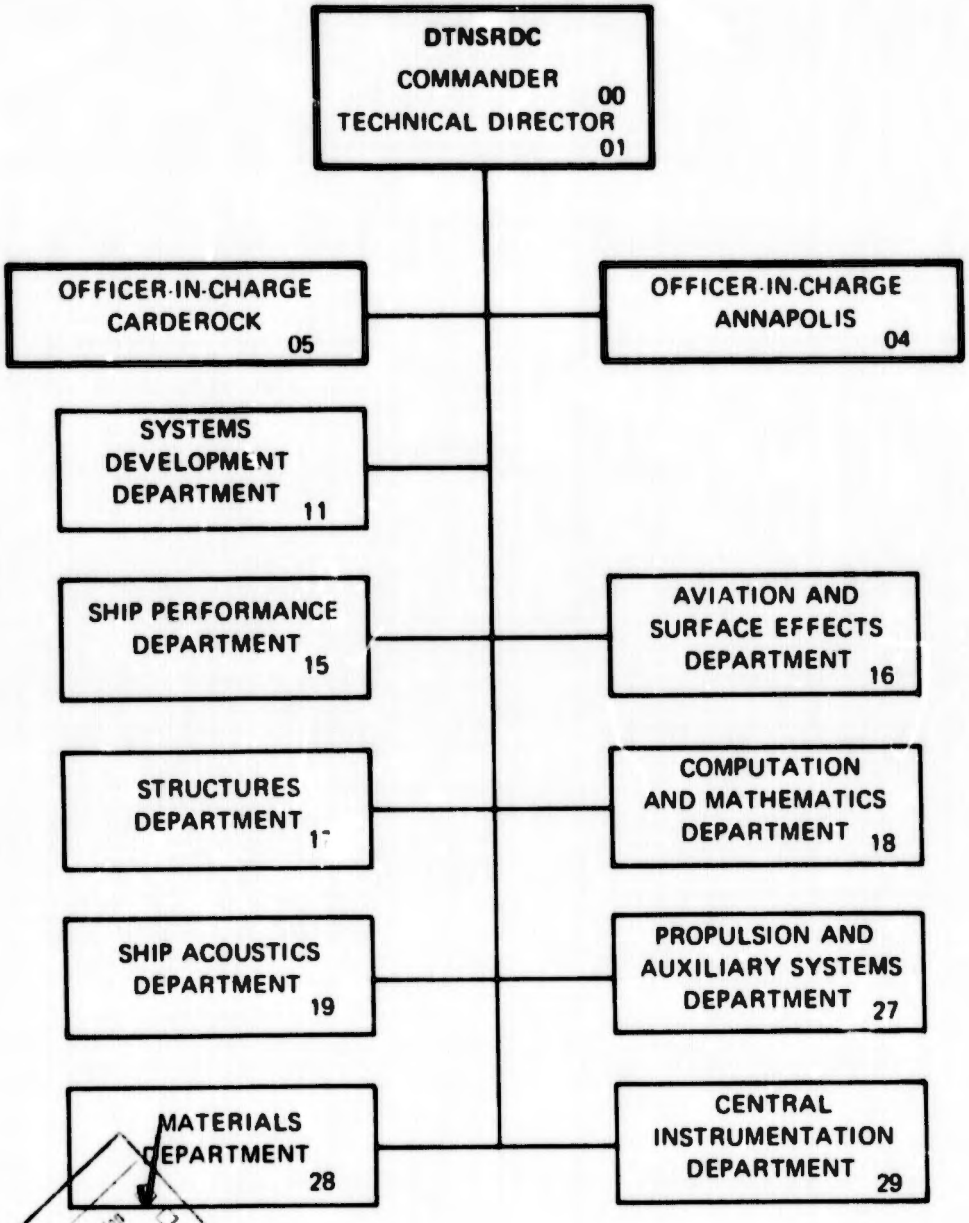

NDW-NSRDC 3960/46 (REV. 8-71)
GPO 888-234

SECURITY CLASSIFICATION OF THIS PAGE (When Data Entered)

REPORT DOCUMENTATION PAGE		READ INSTRUCTIONS BEFORE COMPLETING FORM
1. REPORT NUMBER SPD-363-01	2. GOVT ACCESSION NO.	3. RECIPIENT'S CATALOG NUMBER
4. TITLE (and Subtitle) PERFORMANCE OF CYCLOIDAL PROPELLERS IN CAVITATING ENVIRONMENT		5. TYPE OF REPORT & PERIOD COVERED 6. PERFORMING ORG. REPORT NUMBER
7. AUTHOR(s) G.F. Dobay and M.C. Dickerson		8. CONTRACT OR GRANT NUMBER(s)
9. PERFORMING ORGANIZATION NAME AND ADDRESS David W. Taylor Naval Ship Research Development Center Bethesda, Maryland 20084		10. PROGRAM ELEMENT, PROJECT, TASK AREA & WORK UNIT NUMBERS Subproject S.463.001 Task 12499
11. CONTROLLING OFFICE NAME AND ADDRESS Naval Sea Systems Command Washington D.C. 20350		12. REPORT DATE December 1969 13. NUMBER OF PAGES 61
14. MONITORING AGENCY NAME & ADDRESS(if different from Controlling Office)		15. SECURITY CLASS. (of this report) 15a. DECLASSIFICATION DOWNGRADING SCHEDULE
16. DISTRIBUTION STATEMENT (of this Report) Approved for Public Release: Distribution Unlimited		
17. DISTRIBUTION STATEMENT (of the abstract entered in Block 20, if different from Report)		
18. SUPPLEMENTARY NOTES		
19. KEY WORDS (Continue on reverse side if necessary and identify by block number) Cycloidal propeller, Vertical axis propeller, Torque dynamometer		
20. ABSTRACT (Continue on reverse side if necessary and identify by block number)		

DD FORM 1 JAN 73 1473 EDITION OF 1 NOV 65 IS OBSOLETE
S/N 0102-014-6601

SECURITY CLASSIFICATION OF THIS PAGE (When Data Entered)

NOTATION

Symbol	Definition	Dimensions
b	Blade length	ft
C_L	Lift coefficient	1
c	Blade chord	ft
D	Orbit diameter	ft
g	Acceleration due to gravity	$ft\text{-}sec^{-2}$
h	Depth of submergence at blade half span	ft
J	Advance coefficient, $\frac{V_A}{nD}$	1
K_Q	Torque coefficient, $\frac{Q}{\rho n^2 b D^4}$	1
K_S	Side-force coefficient, $\frac{S}{\rho n^2 b D^3}$	1
K_T	Thrust coefficient, $\frac{T}{\rho n^2 b D^3}$	1
n	Rotational speed	$cycles\text{-}sec^{-1}$
p_a	Ambient pressure, $p_o + \rho gh$	$lb\text{-}ft^{-2}$
p_o	Pressure at air-water interface	$lb\text{-}ft^{-2}$
p_v	Vapor pressure at ambient temperature	$lb\text{-}ft^{-2}$
P	Propeller pitch	ft
P/D	Pitch ratio	1
Q	Torque	lb-ft
R	Resultant force vector, $\vec{S} + \vec{T}$	lb
R_n	Reynolds number, $\frac{c\sqrt{V_A^2 + (\pi nD)^2}}{\nu}$	1
S	Side force	lb
T	Thrust	lb
V_A	Inflow velocity	$ft\text{-}sec^{-1}$
V_L	Local velocity, $\vec{V}_A + \vec{V}_R$	$ft\text{-}sec^{-1}$

V_R	Rotational velocity, πnD	$ft\text{-}sec^{-1}$
α	Blade angle of attack	deg
α_c	Angle of attack due to camber	deg
δ	Angle of resultant force vector (where $\delta = 0^0$ is ahead)	deg
η_o	Propeller efficiency, $\frac{K_T}{K_Q} \cdot \frac{J}{2\pi}$	1
θ	Orbit angle (where $\theta = 90^0$ is ahead)	deg
ν	Kinematic viscosity	$ft^2\text{-}sec^{-1}$
ρ	Density	$lb\text{-}sec^2\text{-}ft^{-4}$
ϕ	Steering angle	deg
σ	Cavitation number, $\frac{p_a - p_v}{\frac{1}{2}\rho V_A^2}$	1
σ_L	Local cavitation number, $\frac{p_a - p_v}{\frac{1}{2}\rho V_L^2}$	1
σ_{LM}	Minimum local cavitation number	1

TABLE OF CONTENTS

LIST OF FIGURES

ADMINISTRATIVE INFORMATION

The work reported herein was funded by the Naval Ship Systems Command, Subproject S.463.001, Task 12499.

INTRODUCTION

The cycloidal, or vertical axis, propeller is a valuable propulsion device due to its unique maneuvering capability. The direction of the resultant force can be controlled and changed to any desired direction normal to the axis of propeller rotation. The history, characteristics, and uses of cycloidal propulsion have been discussed in reference 1.

Most theoretical and experimental work on free-running cycloidal propellers has been undertaken to predict and improve their efficiency. Extensive model data are available, demonstrating maneuvering capabilities,[1*] but very little has been done to investigate the effects of cavitation. Van Manen[2] conducted some tests in a cavitation tunnel but he did not report performance at low cavitation numbers.

This report presents the results of cavitation tests and shows the effects of cavitation on a 9-inch orbital diameter cycloidal propeller in the 24-inch variable-pressure water tunnel[3] at the Naval Ship Research and Development Center. Six blades were used and the blade motion was pure cycloidal. Two pitch ratios and two steering angles for one of the pitch ratios were investigated over a range of advance coefficients and cavitation numbers.

The results of these tests are presented as curves of efficiency, thrust, torque, and side force coefficients as functions of advance coefficient and cavitation number. Photographs and sketches of cavitation observed on the blades are included.

* References are listed on page 21.

EXPERIMENTAL EQUIPMENT

A 9-inch diameter model cycloidal propeller was tested in the 24-inch variable-pressure water tunnel.[3] The propeller (E-1763)* and blades (P-3919) are described in detail in reference 1. The propeller was mounted on four 4-inch modular force gages (block gages). As can be seen in Figure 1, the gages were mounted diagonally but they were oriented to read thrust fore and aft, and side force perpendicular to thrust. Liners were fit into the tunnel nozzles to align the flow with the propeller. The propeller rotor surface was flush with these fairings with only the blades projecting into the flow. A small circular clearance was maintained around the disk of the propeller to allow for the deflection of force gages. The propeller was driven by a motor through a right-angled-drive reduction gear. This unit was mounted on a special hatch on the top of the tunnel. The drive shaft entered the tunnel through an air-tight seal arrangement in the hatch and a differential-reluctance torque dynamometer (E-2020) was located in this shaft just above the propeller.

Outputs from force gages and the torque dynamometer were read on integrating digital volt meters. The instrumentation package included a power supply, an oscillator, a voltage regulator, amplifiers, control units, and a printer.

The tunnel water level was kept at 2.96 feet above the tunnel centerline with propeller, block gages, and dynamometer fully submerged. Openings on the top of the propeller permitted the flooding of the internal mechanism, so that the pressure inside and outside the mechanism was equalized at all times. The tunnel pressure was controlled through the pressure in an air chamber above the water level.

TEST PROCEDURE

Calibration. The torque dynamometer and each block gage were calibrated separately before assembly, using the test instrumentation. Output from the

* Numbers in parentheses refer to NSRDC Drawing numbers.

block gages was monitored while assembling and shimming was applied to avoid a large preload on the gages. In the water tunnel, the propeller blades were removed and another calibration was conducted. Figure 2 shows this assembly outside the tunnel (the universal joint between dynamometer and propeller drive shaft is not shown).

Limited Velocity Survey. A two-point velocity check was made in the modified test section (see Figure 1) with the bladeless unit in place. Water velocity was measured with a pitot tube at two locations: at blade-half span, and at 8 inches below the blade tips, in line with the propeller axis. There was no appreciable difference between velocities measured at the two positions. The freestream velocity throughout the tests was taken as that measured at the second location with the pitot tube.

Establishing Zeros. At the beginning of each test, the propeller was rotated slowly in air and zeros for the force gage instruments were set. No difference in "zeros" was recorded when the propeller was rotated at 1, 2, and 3 rps. It was not practical to check zeros before and after each test because the tunnel was filled with water. However, some checks were made, and a zero shift was observed which will be discussed later in the report.

The torque zero was established with the shaft stationary. Readings from 16 positions in a shaft revolution were taken each day and the mean used as zero.

No-Load Tares. With blades removed, thrust, side force, and torque no-load tares were recorded before and after each change of pitch, over the range of water velocity, rps, and pressure. No-load tares were taken only for the $\phi = 0^{o}$ steering angle. It was assumed that they were the same for the $\phi = 30^{o}$ steering angle.

Propeller Tests. Tests were conducted over a range of advance coefficients and cavitation numbers for each pitch ratio and steering angle.

The range of test conditions is given in Table 1. For each test run, the advance coefficient J was set with the tunnel at atmospheric pressure. Tunnel pressure then was reduced in increments, keeping J constant.

The values of the advance coefficient were computed using the measured pitot tube velocities, in contrast to standard NSRDC test procedures. The standard procedure for screw propellers is to find the advance coefficients for the tunnel data with the use of K_T identity with open-water tests. The method of K_T identity is based on the principle that identical force coefficient values correspond to identical flow conditions (J). As side force is always generated by cycloidal propellers, this principle would have to be applied to the force coefficients based on the resultant force vector, $\vec{R}$. This coefficient is uniquely defined by the magnitudes of the K_T and K_S values [$K_{\vec{R}} \equiv \vec{K}_T + \vec{K}_S$]. A typical comparison of open-water and tunnel data (Figure 3) shows that no $K_{\vec{R}}$ identity can be found throughout the test J range. This indicates that the effect of the tunnel walls on the force data may be severe in a tunnel facility. Using the measured upstream velocities for the computation of J values seems the best method available at the present time.

Table 1

Range of Test Conditions

Pitch Ratio	0.7τ	0.7τ	0.9τ
Steering Angle (Deg)	0	30	0
RPS	6.50	6.50	4.25
Blade Submergence at Half Span (Ft)	2.38	2.38	2.38
Pressure at Half Span (lbs/ft^2)	$250.0 < p_a < 2235.0$	$250.0 < p_a < 2295.0$	$235.0 < p_a < 2240.0$
Velocity ($Ft\text{-}Sec^{-1}$)	$0.90 < V_A < 9.64$	$5.93 < V_A < 9.26$	$1.18 < V_A < 8.93$
Advance Coefficient	$0.18 < J < 1.98$	$1.22 < J < 1.90$	$0.37 < J < 2.80$
Reynolds Number ($\times 10^{-5}$)	$2.15 < R_n < 2.53$	$2.36 < R_n < 2.57$	$1.43 < R_n < 1.90$
Cavitation Number	$2.16 < \sigma < 2772.0$	$2.81 < \sigma < 64.10$	$2.39 < \sigma < 1601.0$
Local Cavitation Number	$0.32 < \sigma_L < 69.73$	$0.36 < \sigma_L$ 61.48	$0.53 < \sigma_L < 19.13$

TEST ACCURACY

In comparing two sets of experimental measurements, it is quite important to establish the relative accuracy of these measurements. This is discussed below, in terms of the test variables.

Upstream Velocity. The accuracy of the upstream velocity measurement for the open-water tests was in the order of

$$-0.2 < \Delta V < +0.2 \text{ ft/sec}$$

The true upstream velocity for the tunnel tests is not known at this time. In lieu of an established method, the pitot tube measurements were used as upstream velocities in the data reduction. The accuracy of these data are in the order of

$$-0.5 < \Delta V < +0.5 \text{ ft/sec}$$

Shaft Revolution. The recording system for rpm measurement was identical for both tests and the error could be in the order of

$$-2.0 < \Delta N < +2.0 \text{ rpm}$$

Instrument Zero. During the tunnel tests, zeros for thrust and side-force measurements were established while the propeller was slowly rotated in air, before each test. Zeros, after tests, were not always taken. The after-test records show a shift in zeros in the negative thrust direction and in the positive side-force direction. The maximum possible error in the force coefficients due to instrument zero shift at the high J range were

$$0 \leq \Delta K_T < +0.1 \quad \text{for } P/D = 0.7\pi ,$$
$$0 \leq \Delta K_T < +0.3 \quad \text{for } P/D = 0.9\pi ,$$
$$0 \geq \Delta K_S > -0.05 \quad \text{for } P/D = 0.7\pi ,$$
$$0 \geq \Delta K_S > -0.10 \quad \text{for } P/D = 0.9\pi .$$

It is believed that the actual error due to zero shift was less than 10 percent of the above maxima

Torque zeros were also shifting but to a much lesser extent. The maximum error was in the order of

$$0 \leq \Delta K_Q < +0.01.$$

During the open-water tests, zeros were recorded both before and after the test runs, and the values averaged. Due to this procedure and to the fact that the zero shift was less during the tests, the maximum error for the force coefficients is expected to be less than half of that for the tunnel tests.

Test No-Loads. Large no-loads are the inherent characteristics of the propeller mechanism design. Especially large torque no-loads result from operating the unit full of water.

The torque and the thrust no-loads obtained for the tunnel tests were similar to those of the open-water tests. In the test J range, they had the following relative values.

$$7\% < \left| \frac{K_{T_{no\text{-}load}}}{K_T} \right| \leq 9\%$$

$$60\% < \left| \frac{K_{Q_{no\text{-}load}}}{K_Q} \right| \leq 70\%$$

Negligible side force no-load values were obtained in the open-water tests, but very large side force no-loads occurred during the tunnel tests, increasing in magnitude with increasing shaft revolution. Over the test J range the tunnel side force no-loads ranged between the relative values of

$$40\% < \left| \frac{K_{S_{no\text{-}loads}}}{K_S} \right| \leq 200\%$$

The same experimental equipment was used in both the open-water and the tunnel tests. There was, however, a difference in the test setup. While in the open-water tests the force gages were not submerged, in the

tunnel tests they were situated in the flooded hatch of the water tunnel (see Figure 1).

It is conceivable that the circulation of the tunnel water, induced by the rotating machinery, could have introduced an asymmetric flow generating a force toward starboard. This supposition is supported by the fact that the side force no-loads were a function of propeller rate of revolution, and relatively insensitive to water speed. Cavitation of the internal propeller mechanism might have occurred at low cavitation numbers. This, however, would not affect the net propeller forces or the net torque, since the corresponding no-loads would have included any such effect (the no-loads were subtracted from the measured test data to obtain the net propeller forces).

PRESENTATION OF TEST RESULTS

1. Tests at Zero Steering Angle

Results obtained with steering angle, $\phi = 0^0$ are shown in Figures 3 through 8. Tests at atmospheric pressure are compared with the open-water curves of reference 1 in Figures 3 and 4. Cavitation test results are shown in Figures 5 and 6. The same data are also shown as functions of the cavitation number in Figures 7 and 8. The cavitation numbers, σ, are based on the speed of advance while the local cavitation numbers, σ_L, are based on the local blade velocities at half-blade-span depth. The smallest local cavitation number, σ_{LM}, is defined as the smallest σ_L value during a blade orbit. For this propeller, σ_{LM} occurs at the orbit angle $\theta = 0^0$; that is, on the port side, looking down and ahead.

2. Tests at 30^0 Steering Angle

Propeller characteristics were also investigated for the 0.7π pitch ratio with the steering angle, ϕ, rotated 30^0 to port. These results are given in Figures 9, 10, and 11. The magnitude of the no-loads is presented in Figures 12 and 13 in coefficient form, so that they could be compared directly with the propeller coefficients.

3. Cavitation Patterns and Inception

Photographs of the cavitating propellers for various values of pitch, steering angle, advance coefficient, and cavitation number may be seen in Figures 14, 15, and 16. The blades in the foreground of these photographs are on the port side of the propeller, and the forward velocity is toward the left.

Each propeller condition shown in the photographs is also depicted in sketches, shown in Figures 17, 18, and 19. Here, the cavitation observed at different orbital blade locations is sketched and the local sigma values are indicated. The blades are not shown at those locations where they were out of the visible range.

The inception of visible cavitation, observed regardless of location, is shown in Figure 20. Visible cavitation means visible to the observer at the tunnel ports. The side of the blades, facing the center of rotation (face), was out of sight during the port-half cycle, while the other side (back) of the blades was not visible during the starboard-half cycle.

DISCUSSION OF TEST RESULTS

Due to the confines of the test facility, it was expected that there would be a difference between the tunnel data and the open-water characteristic curves. Also, the large side force no-loads and zero drift, discussed under Test Accuracy, make the tunnel test results less accurate than the results from the open-water tests. As mentioned earlier, the exact value of the upstream velocity was not known for the tunnel data. However, due to the location of the pitot tube, it is believed that the pitot tube velocities do represent the average flow velocity into the propeller.

1. Test Results at Zero Steering Angle

Comparison of the Open-Water and Tunnel Data. The tunnel test data (Figures 3 and 4) appear to have the same trend but different values at corresponding advance coefficients from those obtained during open-water tests. As can be seen, in general, larger torque coefficients, smaller thrust coefficients, and larger negative side force coefficients result

from the tunnel tests. If water velocities from K_T identity, instead of from the pitot tube measurement were used in computing the tunnel advance coefficients, even larger discrepancies would exist between the torque coefficients and between the side force coefficients.

The fact that the side force no-loads in the tunnel (Figure 12) are in the same direction as the side forces obtained during the test (Figures 3 and 4) indicates that the flow into the propeller was different in the two test facilities. Further proof of this is that the magnitudes of the resultant force vector, R, have practically the same value for both test facilities at ϕ = 0 deg. The direction of the resultant forces differ, however. As an example, for J = 0, at the nominal zero steering angle ($\phi = 0^0$) the comparable values are

open-water tests	$\delta \simeq -3^0$
tunnel tests	$\delta \simeq -18^0$

Here δ is the angle between the resultant force vector and the positive thrust direction, positive counterclockwise ($\delta = \arctan \frac{K_S}{K_T}$).

Tunnel test results of cycloidal propellers were recently reported by the Kryloff Shipbuilding Research Institute.[5] A rectangular cross-section closed-jet tunnel was used and the tests were apparently conducted at atmospheric tunnel pressure. In Figure 2 of this paper, comparison is made between the Institute's test results and the open-water test results of NSRDC.[6] Excellent agreement is shown between the torque coefficients, but there is a 10-to-20 percent difference between the thrust coefficients. The open-water thrust results[6] are consistently lower than those of the Kryloff tunnel. The NSRDC tunnel results also show good agreement for the torque with the same open-water tests, but the thrusts are consistently lower than those of the open-water tests.[6] The NSRDC tunnel has essentially an open-jet test section.

The text of the Kryloff paper does not mention any possible wall effects on their data. It is quite apparent, however, that the flow boundaries did have an effect of similar magnitude on the propeller thrust in both tunnel facilities, but in opposite direction. Unfortunately, no side force measurements were reported for the Kryloff tests. One would

expect that the direction of the resultant force would also rotate opposite to the direction of the NSRDC tunnel tests. It would be desirable to investigate further this apparent facility effect on the direction of the resultant force vector, by direct comparison of propeller test results from an open and a closed-jet test section.

Cavitation Test Results. The discrepancy between the open-water and tunnel data (atmospheric pressure) has to be resolved. The main purposes of the tunnel tests, however, was to obtain the propeller characteristics in cavitating environment. As comparison will be made between test data obtained in the same (tunnel) facility, the relative performance degradation would be expected to be valid, irrespective of the facility effects.

The effect of cavitation on the force coefficients of a cycloidal propeller is not unlike that for conventional propellers: there are, however, differences. At 0.7π pitch ratio (Figure 5) a decrease in tunnel cavitation number causes an increase in torque and a decrease in thrust and in side force. This is not the case for the 0.9π pitch ratio (Figure 6). Here, over the significant J range, efficiency increases with decreasing cavitation number due primarily to the decrease in torque required. The change in forces is minimal.

A clearer picture may be obtained if one examines the coefficients as functions of cavitation number (Figures 7 and 8). In comparing the torque coefficients for the two pitch ratios (Figures 7a and 8a), it can be observed that in the significant J range, the low pitch propeller ($1.3 < J < 1.9$) requires a sizeable increase in torque with decreasing cavitation number. The K_Q curves for the high pitch in the $2.0 < J < 2.6$ range are decreasing with decreasing cavitation number, similar to the $J = 2.801$ curve (Figure 8a). The side force and thrust curves remain relatively constant for both propellers over the explored cavitation number range. Consequently, for the above J ranges, the efficiency increases with cavitation number for the high pitch and decreases for the low pitch.

In the case of cycloidal blade motion, the blade loading varies throughout a cycle of rotation, influenced by the change in effective angle of attack, velocity of blade oscillation and local blade velocity. It is believed that the cavitation number, based on local blade velocity, is a more meaningful indicator of the cavitating performance of the propeller than cavitation number based on forward velocity. The minimum value of the local σ_L occurs at 90^0 to port for these propellers ($\theta = 0^0$). The values at half-blade span depth of the minimum local cavitation numbers (σ_{LM}) are shown on the thrust coefficient curves (Figures 7d and 8d). One may note that for the same forward speed (σ) and thrust coefficient (K_T), the σ_{LM} values are much higher for the high pitch propeller. The difference in performance is illustrated in Table 2. There is no apparent performance degradation with σ in the high pitch case. Relative performance degradation. due to cavitation, could be inferred from the relative values of the local cavitation numbers.

Table 2

P/D	J	K_T	η (σ = 5.0)	η (σ -> 25.0)
0.7π	1.46	1.2	0.43	0.52
0.9π	2.14	1.2	0.52	0.51

2. Test Results at 30^0 Steering Angle (0.7π Pitch Ratio)

The test data acquisition accuracy is the same as that of the zero steering angle tests. The facility effect on the force results should, however, be much greater for $\phi = 30^0$ than it was for $\phi = 0^0$.

Comparison of the Open-Water and Tunnel Data (Atmospheric Pressure). The trend of the water tunnel data is the same as that of the open-water tests (Figure 9). There is a large difference in the K_S values obtained in the two facilities, similar in magnitude to the $\phi = 0^0$ tests (Figure 4).

For the $\phi = 30^0$ steering angle, the water tunnel K_T values are somewhat higher than those obtained in open water. THe direction of the resultant force obtained from the tunnel tests is such that it lags behind that of the open-water data, up to the zero thrust J value. It is interesting to note that for $\phi = 30^0$ the angles of the resultant force vector, δ, obtained from the tunnel tests, are in much closer agreement with the predicted δ (see Figure 31a of reference 1) over the test J range, than are those from the open-water tests. This may be a coincidence since for the $\phi = 0^0$ case, larger negative δ values were obtained from the tunnel tests than from the open-water tests, at low J values (Note: the predicted value, of course, is $\delta = 0$).

The magnitude of the resultant force, obtained from the tunnel tests, is less than that from open-water tests, principally due to the smaller positive value obtained for the side force. One can conclude the following: within the range of the test variables

$$(K_S)_{tunnel} < (K_S)_{open\text{-}water}$$

$$(\delta)_{tunnel} < (\delta)_{open\text{-}water}$$

$$(K_T)_{tunnel} \simeq (K_T)_{open\text{-}water}$$

$$(K_Q)_{tunnel} \simeq (K_Q)_{open\text{-}water}$$

The large, nearly constant difference between $(K_S)_{tunnel}$ and $(K_S)_{open\text{-}water}$ over the J range indicates an effective angle of attack change of the blades due to the presence of the tunnel boundaries.

Cavitation Tests. The effect of cavitation on the force coefficients appears to be much greater for the $\phi = 30^0$ tests (Figure 10) than it was for the $\phi = 0^0$ tests (Figure 5). Both the K_T and K_S values decrease considerably with cavitation number (Figure 11), much more radically than for the $\phi = 0^0$ tests (Figure 7). That cavitation is more extensive at $\phi = 30^0$ than at $\phi = 0^0$ is also indicated by the K_Q curve (Figure 11). After an initial hump the K_Q values also decrease with decreasing σ.

3. Cavitation Patterns and Inception

The appearance of cavitation on a cycloidal propeller is unlike that for a conventional screw propeller in uniform flow. The local flow velocity into the blade changes continuously throughout each cycle of rotation in both magnitude and direction. Also, the flow encountered in the aft portion of a cycle is not uniform due to the wake of the forward blades.

Photographs of the propellers, at various stages of cavitation, are shown in Figures 14 through 16. Unless one looks at them with a trained eye, it is very difficult to observe cavitation in these figures. Sketches were made of cavitation, depicted from visual observation. The viewing ports were on the port side of the propeller. For ease of discussion, the two sides of the blades are defined as follows. The sides of the propeller blades facing toward the center of rotation will be called the face of the blades and the other, the back of the blades.

As a consequence of the cycloidal blade motion, the blades are subject to both positive and negative angles of attack over a cycle of revolution. Here, positive angle of attack is defined as that producing a lift force directed away from the center of rotation (positive lift). The following holds true with this definition:

Sign of α	$\phi = 0^o$	$\phi = 30^o$
+	$0^o \leq \theta \leq 180^o$	$330^o \leq \theta \leq 150^o$
-	$180^o \leq \theta < 360^o$	$150^o < \theta < 330^o$

In the case of symmetric blade sections, the sign of the generated lift force is synonymous to the sign of α. It is somewhat more difficult to determine which side is the suction, or low pressure, side of the blades when they are cambered.

In the NSRDC test series, cambered blades were used. The blades had circular-arc camber, with a radius R = 4.5 inches.[1] Due to the large thickness ratio and the blade outline, the calculated value of the zero lift angle (or apparent angle of attack due to camber) for these blades can only be considered an estimate. This value is estimated to be

$$\alpha_c = -\alpha\big|_{C_L=0} \approx +3^0$$

The magnitude of the blade angle, $|\alpha|$, decreases with increasing J, and increases with increasing pitch ratio. Due to the uncertainty of the zero lift angle, the exact J value at which the camber compensates for some of the negative angles of attack is not known. It is very likely, however, that at high J values, positive lift was generated by the blades in the $270^0 < \theta \leq 0^0$ quadrant ($\phi = 0^0$).

Cavitation Patterns (0.7π Pitch Ratio)

$\phi = 0^0$: When the propeller is lightly loaded (small values of K_T and K_S) at high J values (ex: Figure 17a), cavitation of the blades is not excessive in spite of the low cavitation numbers. The effective angle of attack ($\alpha + \alpha_c$) for the blades is small. Close to the maximum efficiency of the propeller (Figure 17b) considerable cavitation exists on the blades, due to the high effective blade angles and low cavitation numbers. This results in about a 15-percent reduction of thrust and a 24-percent increase in the required torque (Figure 5).

The bubble cavitation, appearing on the back of the blade at high J values (Figures 17a and 17b), indicates that the back of the blades did become the suction side in the $270^0 < \theta < 0^0$ quadrant. The faces of the blades were cavitating in the $180^0 < \theta < 270^0$ quadrant as they are the low-pressure sides in that quadrant. No cavitation would be expected on the faces in the $270^0 < \theta < 90^0$ quadrant as they are the high-pressure side of the blades. For the same reason, no cavitation is expected on the back in the quadrant $180^0 < \theta < 270^0$.

At even higher blade loadings (Figures 17c and 17d), the tip vortex cavitation becomes more pronounced (high negative angles of attack in the $180 \leq \theta \leq 270^0$ quadrant). This, and some bubble cavitation on the blade persist at low J values, for cavitation numbers up to $\sigma \approx 35.0$. At these low J values, cavitation has minimal effect on the forces; it mainly increases the required torque (see Figure 7).

$\phi = 30^0$: The same general trend in blade cavitation can be observed for nonzero steering angles as for the zero steering angle (Figures 18a through 18d). More cavitation exists throughout the J range as the propeller loadings vary from moderate to heavy. The direction of the resultant force varied over the test J range between

$$55^0 < \delta < 95^0$$

to the port, measured from straight-ahead.

One should note the excessive back cavitation at low J values (Figures 18c and 18d) due to the large positive angles of attack in the $30^0 < \cdot < 120^0$ quadrant. This amount of cavitation would take place only at the initial stage of changing course. As the craft would advance in the direction of the resultant force, it is expected that the amount of cavitation on the blades would decrease.

Cavitation Patterns (0.9π Pitch Ratio)

It was mentioned earlier that the effect of cavitation number on the force coefficients appeared to be less severe for the 0.9π pitch propeller than for the 0.7π pitch propeller (Figure 6). This is the result of much less cavitation on the propeller blades at comparable loadings (Figures 19a through 19d). At close to optimum efficiency (Figure 19b) almost no blade cavitation was observed at the 0.9π pitch, while considerable blade cavitation existed on the 0.7π pitch (Figure 17b), although the blade loading was somewhat higher for the 0.9π pitch. The trend in cavitation, as J is reduced, is the same for the two pitch ratios.

In general, there are two opposing influences of increasing the pitch ratio of a cycloidal propeller.

The optimum efficiency of the propeller is shifted toward higher J values, resulting in higher σ_{LM} values at the same forward speed (or σ) for a specific K_T value. This tends to reduce the amount of blade cavitation.

The other influence of increasing pitch ratio is the increase in the blade angles of attack (α) at corresponding orbit angles (θ) over a blade cycle (J = constant). This is a direct consequence of cycloidal blade motion. The danger of flow separation on the low-pressure sides of the blades is thus increased. Also, cavitation of the blades may begin earlier (at higher local σ_{LM} values) due to the higher blade angles.

The type of propeller blade used will determine which of the two effects dominate the cavitation characteristics of the propeller.

It seems that the type of blade[1] used in the tests has good cavitation characteristics, and the increase in angle of attack due to higher (0.9π) pitch ratio did not raise radically the σ_{LM} value, at which the blade would cavitate. One cannot say, however, that a higher than 0.9π pitch ratio propeller would have still better cavitation characteristics.

One may note that for the 0.9π pitch propeller, there is a J range ($2.1 < J < 2.6$) where the efficiency actually increases as the cavitation number (σ) decreases (Figure 6). Although this could not be observed, it could be inferred from the foregoing that it was due to blade cavitation on the face side in the $270^0 < \theta < 0^0$ quadrant. In this quadrant the blade angle (α) is negative and could be sufficiently large at these high J values to cause a slight negative effective angle of attack on the cambered blade sections.

Cavitation Inception

The observable cavitation inception curves (Figures 20a and 20b) show that much higher craft velocities can be obtained with the high pitch propeller than with the lower pitch propeller before inception takes place. This result again points to the fortunate selection of the blade section, but it could not be said how far this trend would continue with increasing pitch ratio.

The inception curves also show (Figure 20c) that a nonzero steering angle (ϕ) will increase the value of the cavitation number for inception over that of $\phi = 0^0$ if the craft motion is straight-ahead. This is especially true for tip vortex and face cavitation, and is caused by the high blade loading.

4. Full-Scale Application

There is a minimal amount of information available on problems encountered in the operation of naval craft. However, there are some

indications that loss in efficiency or directional control problems are sometimes encountered. In order to illustrate how the test results reported here could provide an insight to some full-scale propulsion problems, two German minesweepers are taken as examples:

A. World War II Minesweeper (German)[7]

Approximate Description of the Cycloidal Propulsion:

Number of Propellers: 2

Propeller Diameter: D = 55.1 inches

Number of Blades: Z = 7

Blade Length: b = 34.25 inches

P/D = 0.73

Water Depth at Blade Root: h = 21.0 inches

Design J = 1.932

Ship Speed: V_s = 20 knots

Shaft rpm: N = 230

Possible Cavitation of the Propellers

At design ship speed, the ship cavitation number, σ, is 2.1 at the tip of the blades. The local minimum blade cavitation number varies along the blade length (at design speed) between

$$0.517 < \sigma_{LM} < 0.563$$

At the pitch ratio of 0.73π, the design advance coefficient (J = 1.932) roughly corresponds to the maximum efficiency of this propeller. One could compare this condition to the performance data of the 0.7π pitch ratio model propeller at J = 1.668 (Figures 7 and 17b). It can be seen that considerable blade cavitation can be expected on these propellers, possibly causing the ship to slow down.

B. German Naval Craft*

Approximate Description of the Cycloidal Propulsion:

Number of Propellers: 2

Propeller Diameter: 63 inches

* Unpublished information received from the Naval Ship Engineering Center.

Number of Blades: 6

Blade Length: b = 39.4 inches

P/D = 0.82π

Water Depth at Blade Root: h = 24 inches

Design J = 2.013

Ship Speed: V_S = 24 knots

Shaft rpm: N = 230

Possible Cavitation of the Propellers

At design ship speed, the ship cavitation number, σ, is 1.5 at the tip of the blades. The local minimum blade cavitation number varies along the blade at design speed between

$$0.391 < \sigma_{LM} < 0.440$$

At the design pitch (P/D = 0.82π) this propeller operates roughly at peak efficiency for the given design J value.

The expected cavitation of this propeller can be judged by the results of the 0.9π pitch ratio model tests, at J ~ 2.10 (Figures 8 and 19b). As both the full-scale cavitation number and pitch ratio are lower than those of the model tests, more cavitation than shown in Figure 19b can be expected full-scale. The trend of the test results indicates that, although the required torque may remain relatively insensitive to cavitation, there could be a considerable reduction in available thrust, and the ship would slow down.

Based on the model tests, the full-scale propellers in both examples could well have suffered from both cavitation erosion (bubble cavitation) and performance degradation. This anticipation is less definite for the higher pitch full-scale propeller as the higher pitch model propeller has been affected by cavitation to a much lesser degree than the low pitch model.

CONCLUSIONS AND RECOMMENDATIONS

The change in performance characteristics of cycloidal propellers due to cavitation is quite similar to that of conventional screw propellers. In

general, the available thrust decreases and the required torque increases with decreasing cavitation number. There are, however, important differences which need to be explored to a fuller extent.

There is a striking improvement in performance of the 0.9π pitch propeller to that of the 0.7π pitch propeller at the same loading and cavitation number. Further cavitation tests should explore this trend further, using higher than π pitch ratios. The higher than π pitch ratio propellers operate at optimum efficiency at high J values. Thus, they can be thought of as high-speed propulsion devices. If cavitation tests prove them useful at low σ values, they would be competitive candidates for the propulsion of novel high-speed naval craft along with the waterjet and supercavitating propellers.

The type of cavitation on the propeller blades changes continuously throughout each cycle of revolution. This cyclic loading could cause blade fatigue problems. Blade force and fluctuating torque measurements should be made under cavitating conditions.

It appears that in the current usage of cycloidal propulsion, the propellers normally operate in cavitating environment. Since there was a considerable performance degradation of the low pitch propeller model, it is strongly recommended that cavitation tests be conducted of future designs for the better prediction of full-scale performance.

From this first series of tests, facility effects appear to have a strong influence on the test data. Only relative (to water tunnel tests) performance degradation can thus be predicted. It is recommended that the effect of the tunnel facility on propeller performance be further explored, by repeating some of these tests in a larger water tunnel.

REFERENCES

1. Ficken, N. L. and Dickerson, Mary C., "Experimental Performance and Steering Characteristics of Cycloidal Propellers," Naval Ship Research and Development Center Report 2983 (Aug 1969).

2. Van Manen, J. D., "Results of Systematic Tests with Vertical Axis Propellers," International Shipbuilding Progress, Vol. 13 (Dec 1966), pp. 382-398.

3. Brownell, W. F. and Miller, M. L., "Hydromechanics Cavitation Research Facilities and Techniques in Use at the David Taylor Model Basin," David Taylor Model Basin Report 1856 (Oct 1964).

4. McKillop, J. A., "A Study of the Flow Through a Vertical Axis Propeller," Engineering Research Associates Report 60/1 (Apr 1965).

5. Ibragimova, T. B. and Roussetsky, A. A., "Some Distinguishing Features of Cycloidal Propeller Hydrodynamic Performance," Paper presented before the 12th ITTC, Rome (1969).

6. Ficken, N. L., "Conditions for the Maximum Efficiency Operation of Cycloidal Propellers," Paper presented before the Chesapeake Section, SNAME (Apr 1966).

7. Klemmer, E. T. and Johnson, P. K., "Trials Conducted on a German P130 Class Minesweeper Equipped with Voith-Schneider Cycloidal Propellers," David Taylor Model Basin Report 649 (Dec 1948).

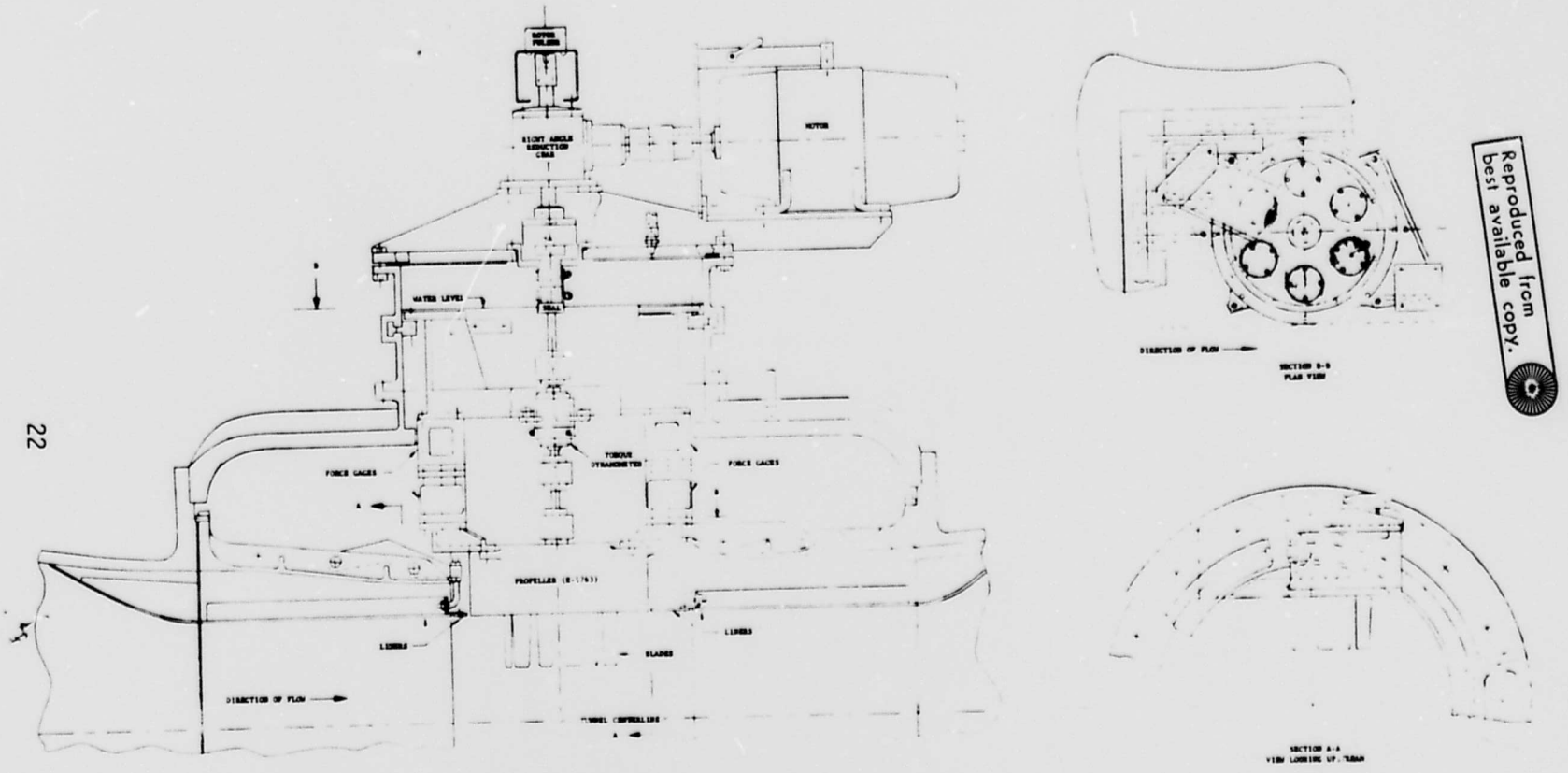

Figure 1 - Schematic of Installation in Variable-Pressure Water Tunnel

PSD 329008

Figure 2 - Propeller in Assembly for Calibration

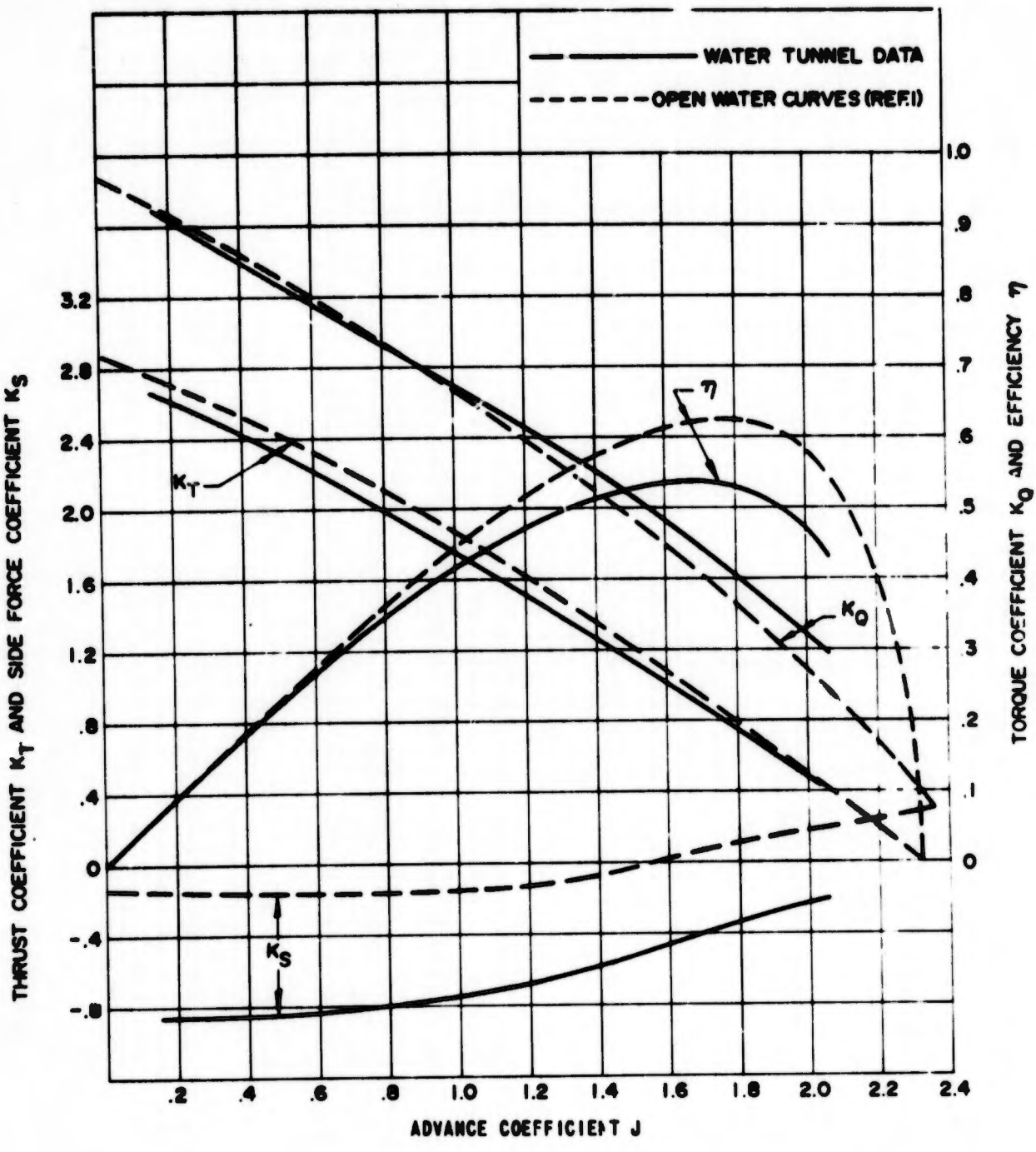

Figure 3 - Noncavitating Propeller Characteristics for 0.7π Pitch Ratio and Zero Steering Angle

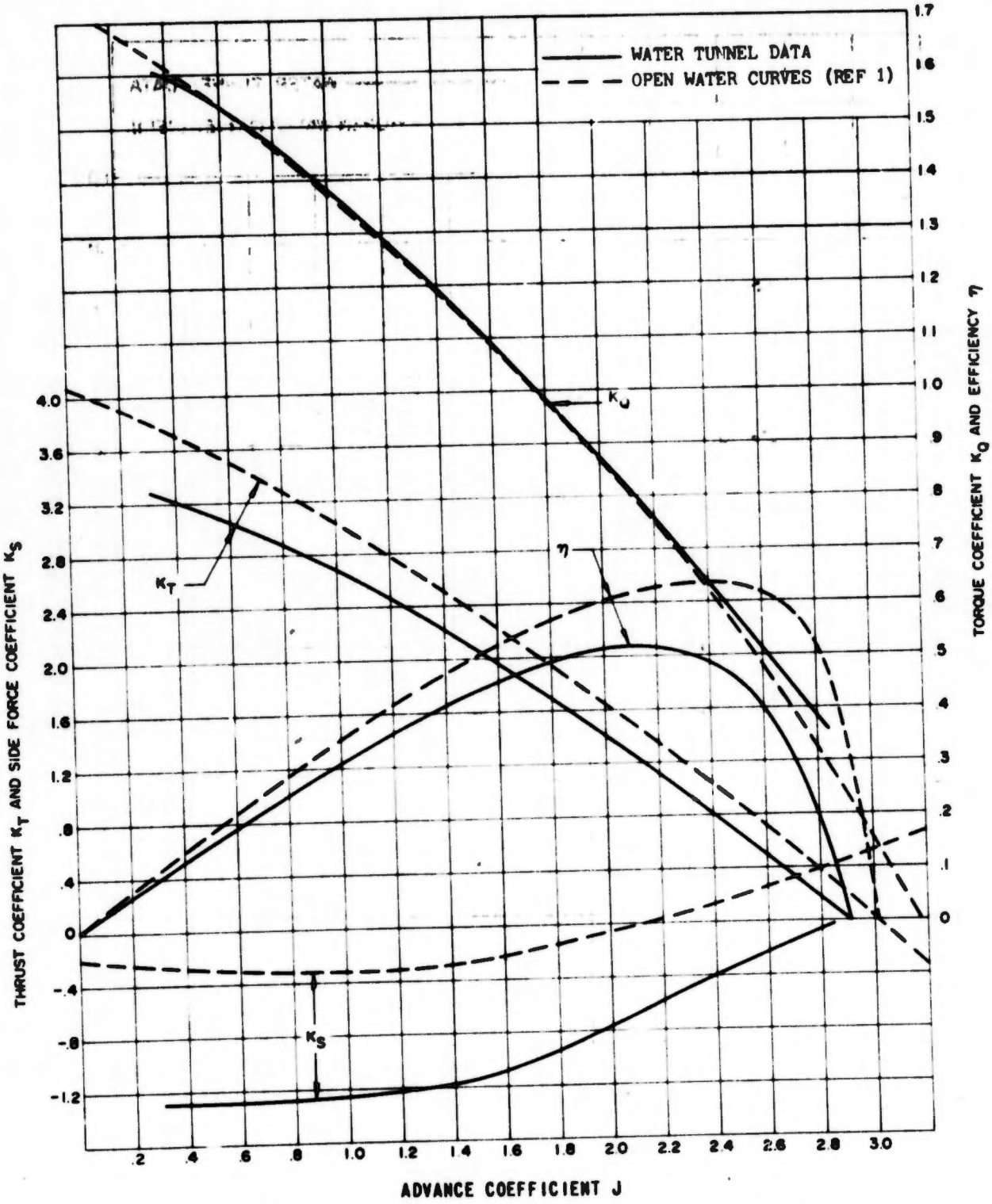

Figure 4 - Noncavitating Propeller Characteristics for 0.9π Pitch Ratio and Zero Steering Angle

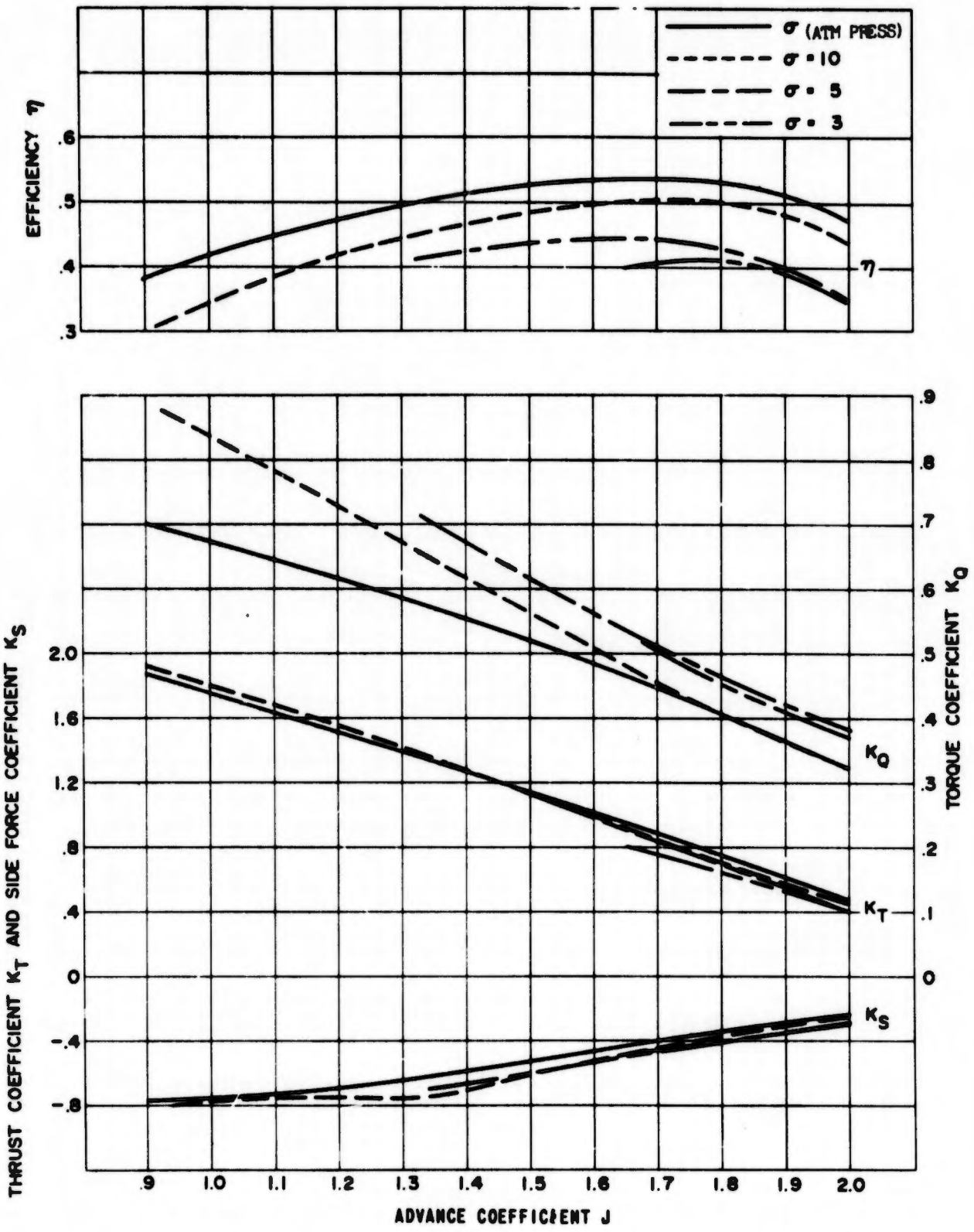

Figure 5 - Propeller Characteristics with Cavitation for 0.7π Pitch Ratio and Zero Steering Angle

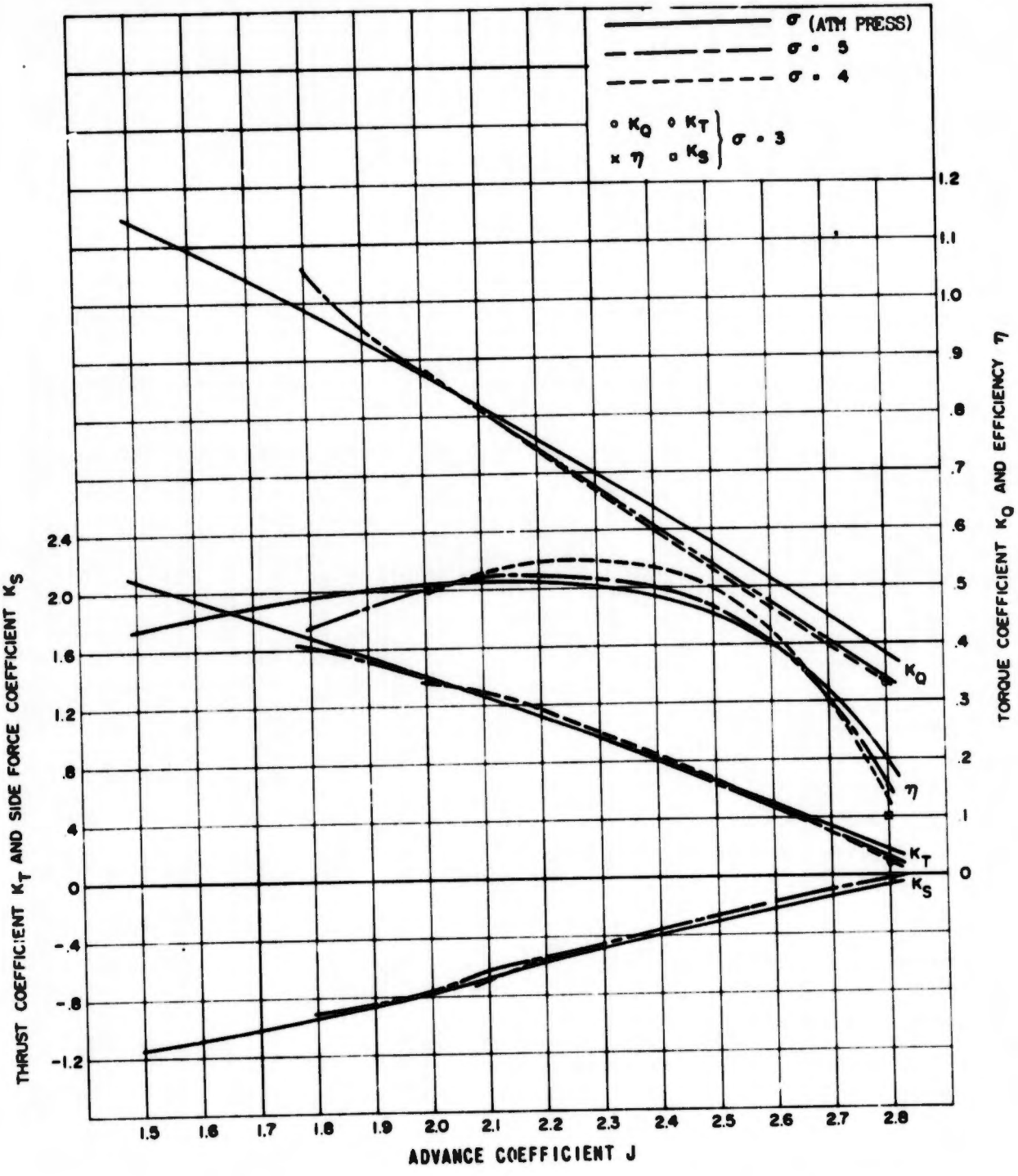

Figure 6 - Propeller Characteristics with Cavitation for 0.9π Pitch Ratio and Zero Steering Angle

Figure 7 - Propeller Characteristics with Varying Cavitation Number for 0.7π Pitch Ratio and Zero Steering Angle

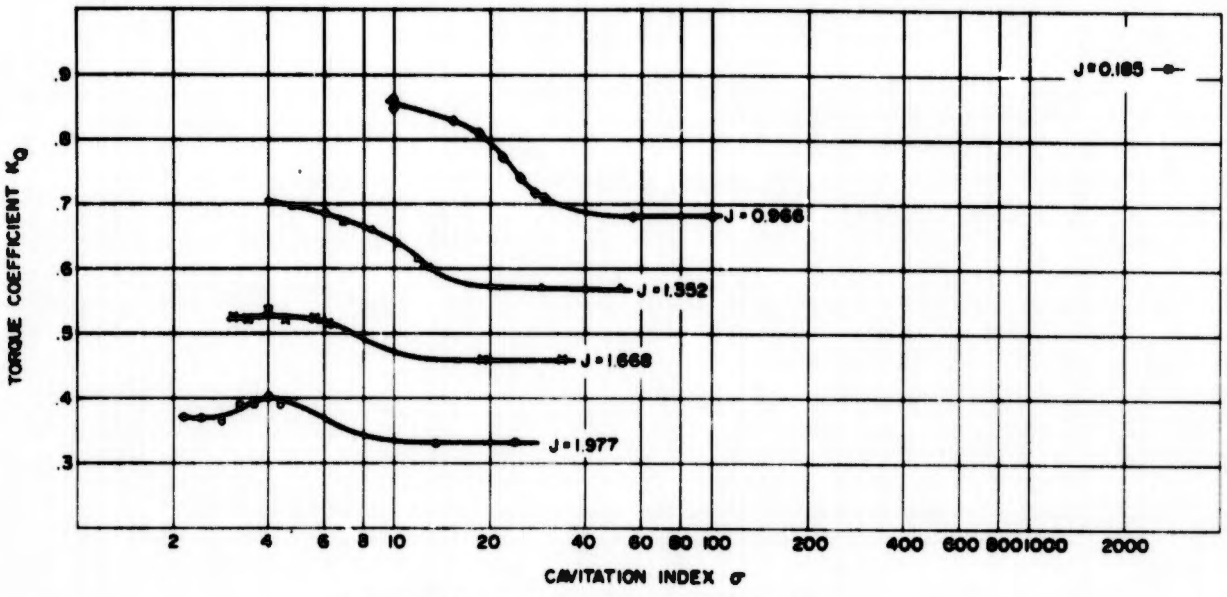

Figure 7a - Torque Coefficients

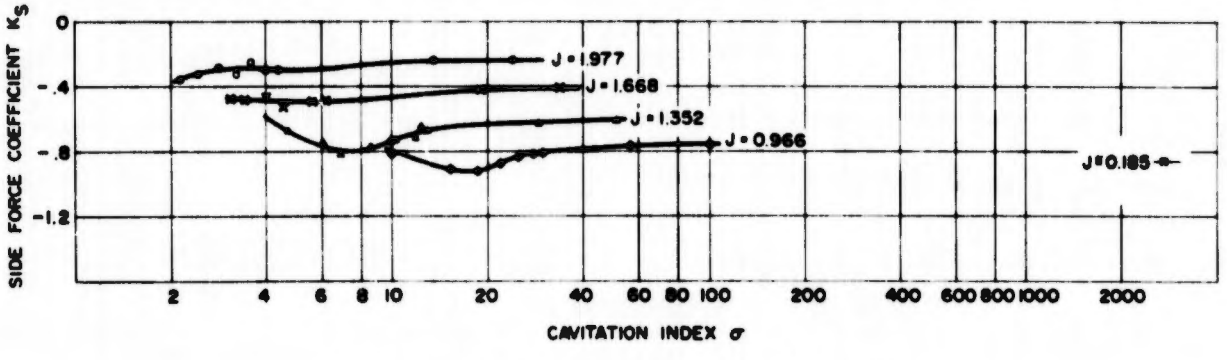

Figure 7b - Side Force Coefficients

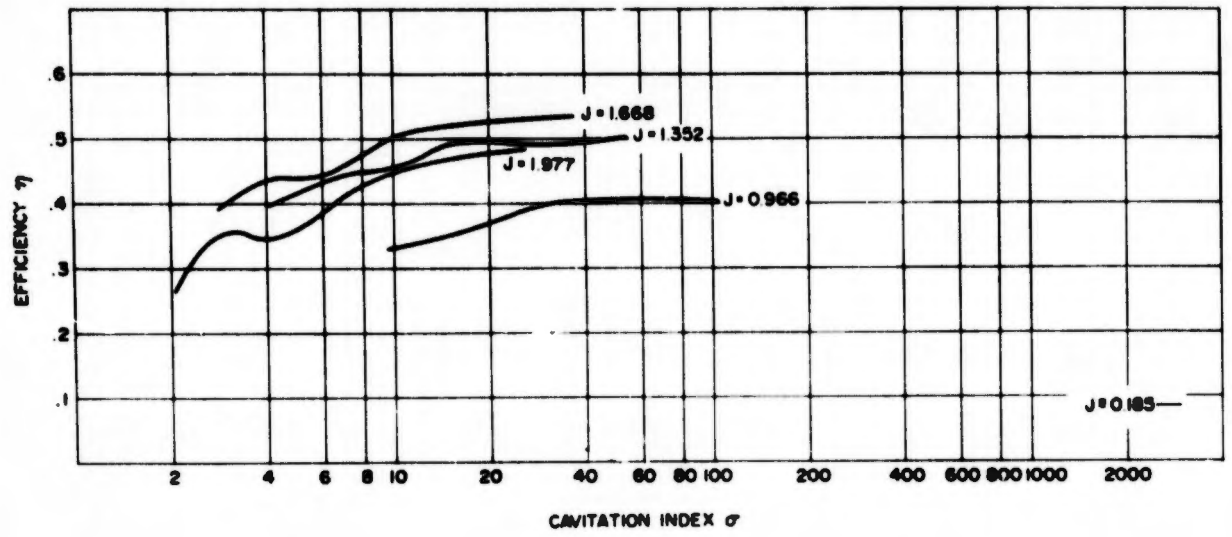

Figure 7c - Efficiency (P/D = 0.7π, ϕ = 0)

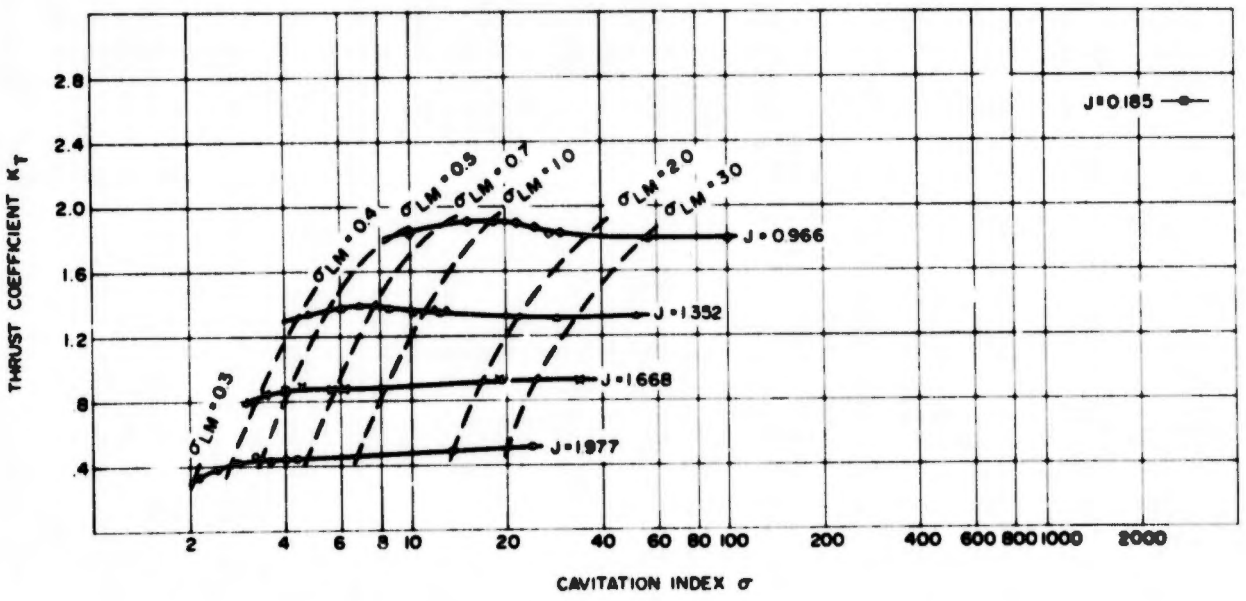

Figure 7d - Thrust Coefficients (P/D = 0.7π, ϕ = 0)

Figure 8 - Propeller Characteristics with Varying Cavitation Number for 0.9π Pitch Ratio and Zero Steering Angle

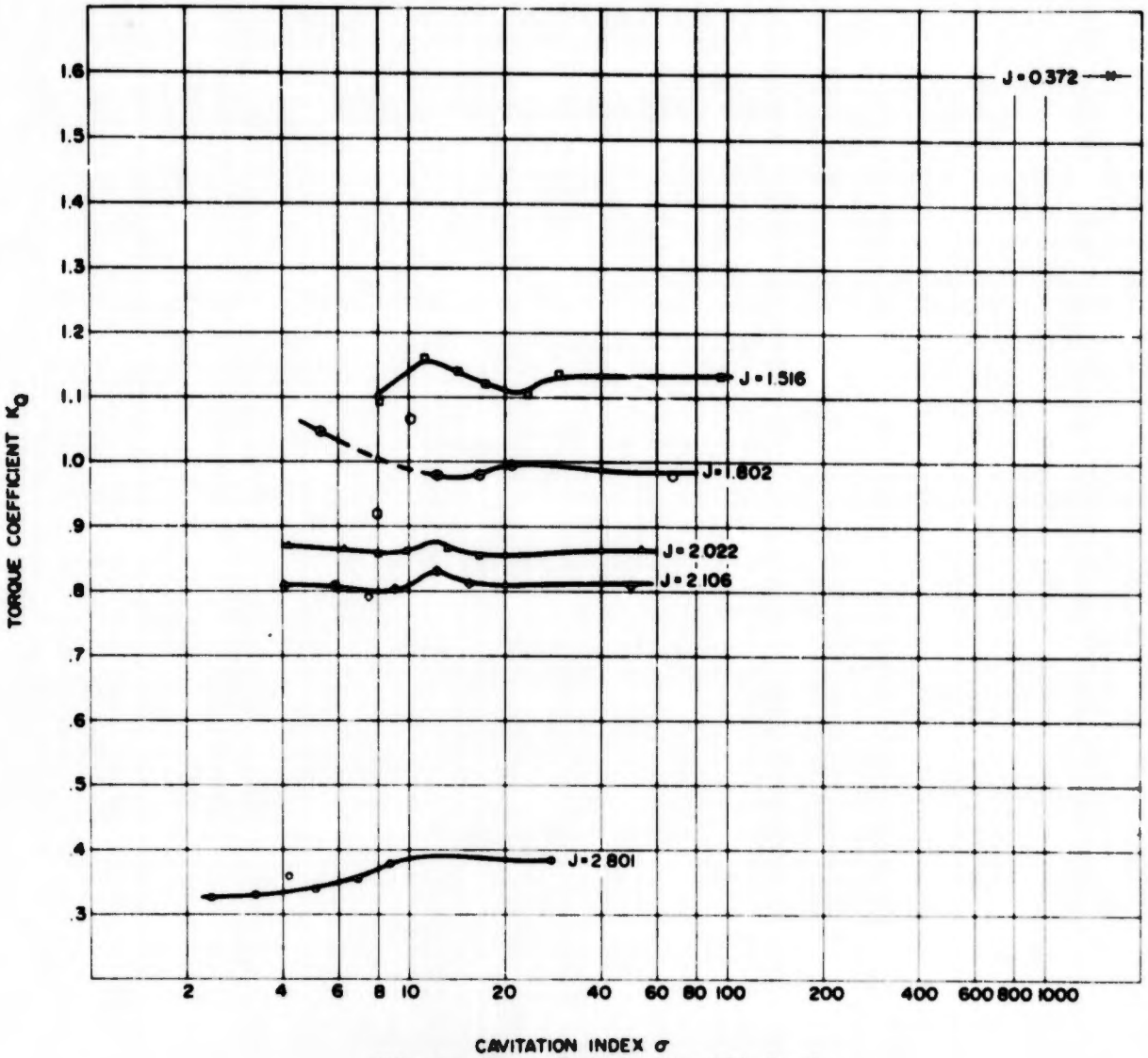

Figure 8a - Torque Coefficients

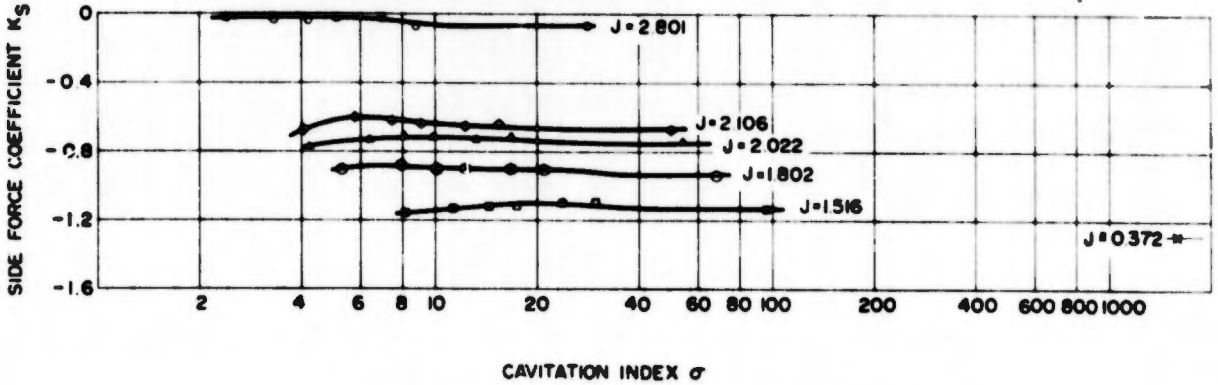

Figure 8b - Side Force Coefficients

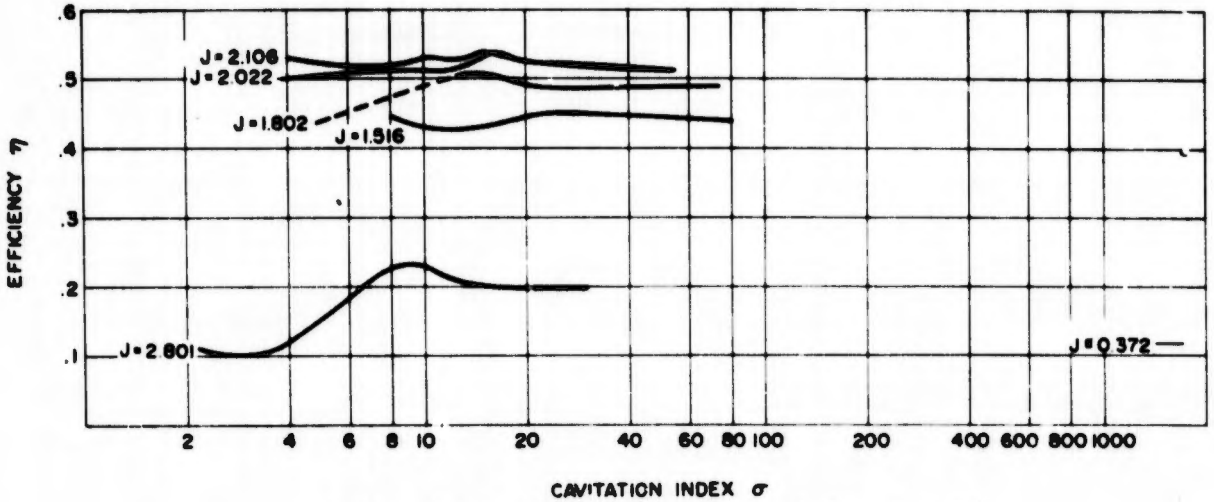

Figure 8c - Efficiency (P/D = 0.9π, ϕ = 0)

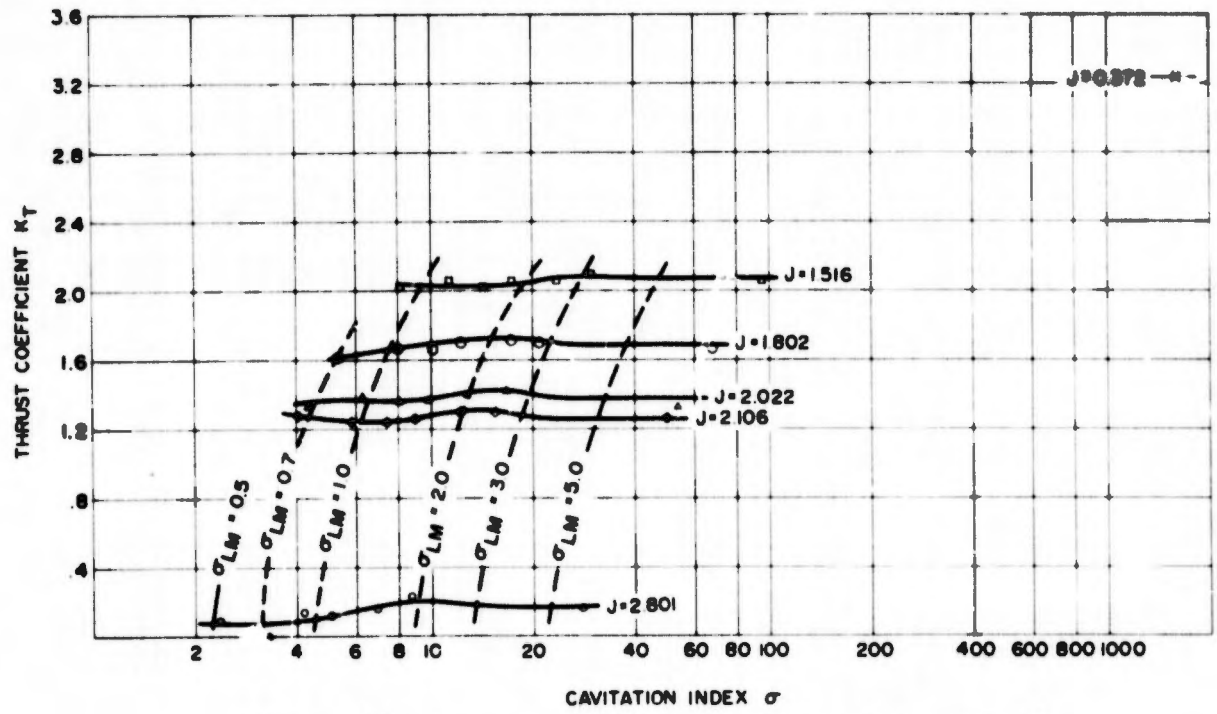

Figure 8d - Thrust Coefficients (P/D = 0.9π, ϕ = 0)

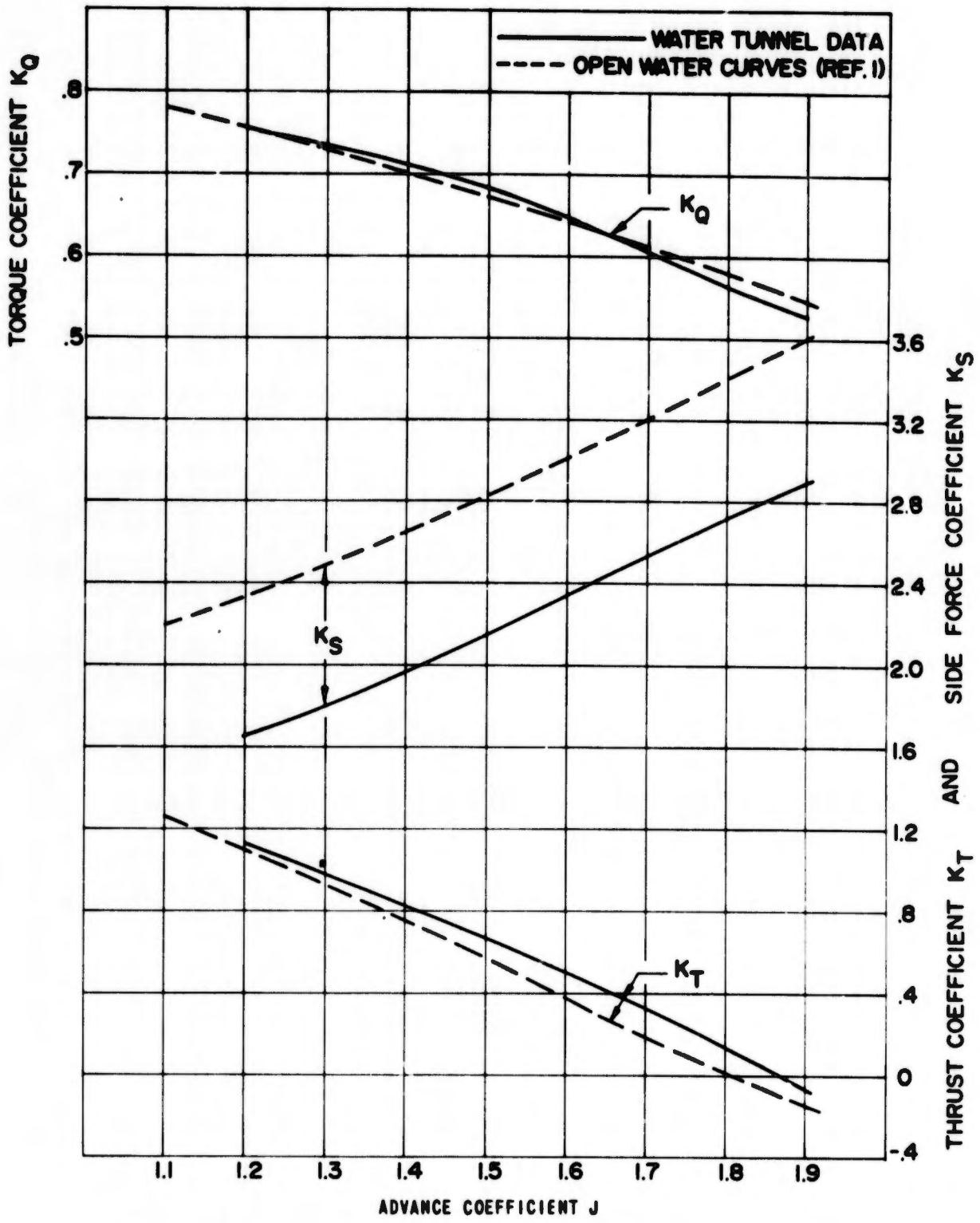

Figure 9 - Noncavitating Propeller Characteristics for 0.7π Pitch Ratio and 30-Degree Steering Angle

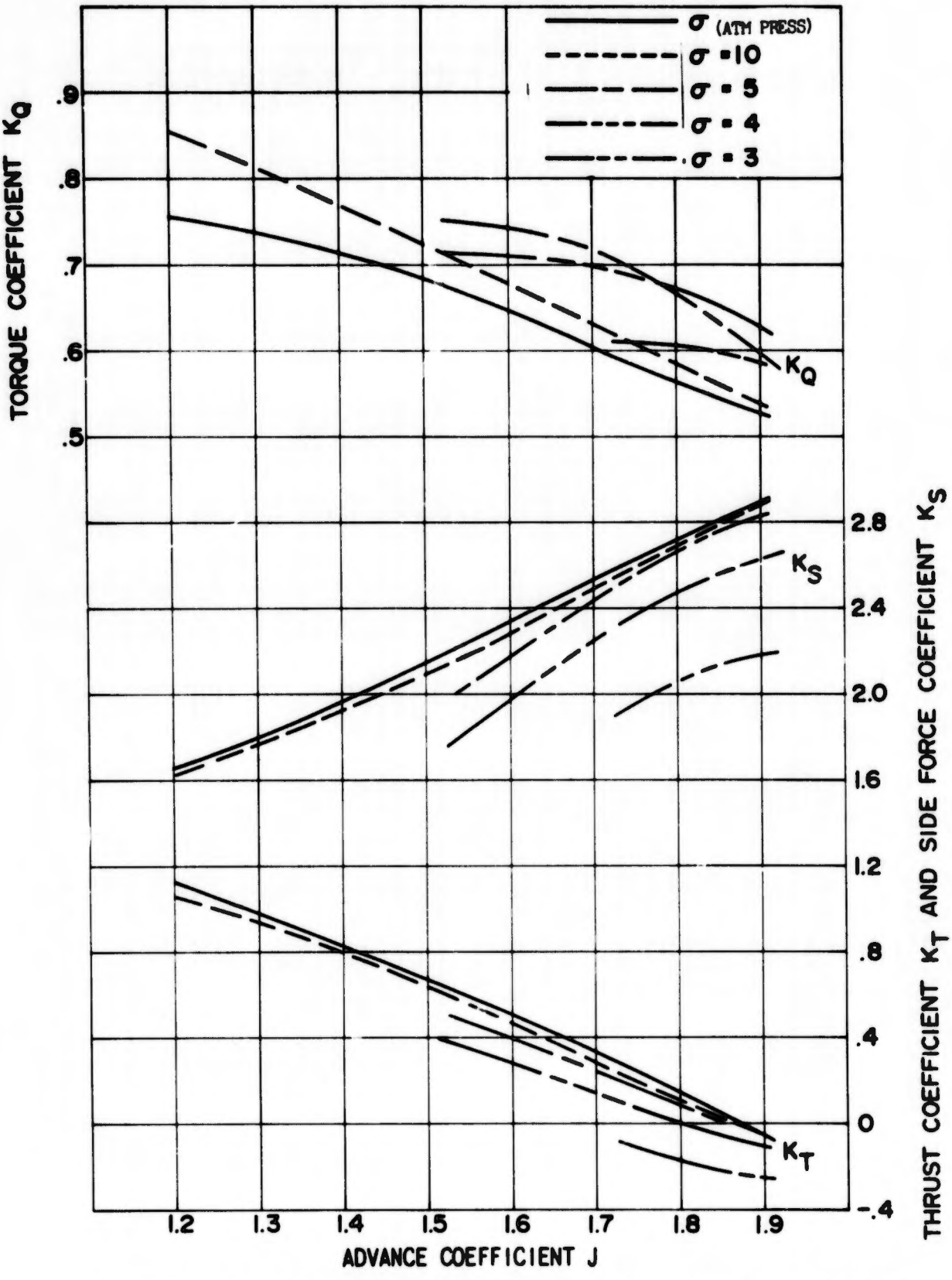

Figure 10 - Propeller Characteristics with Cavitation for 0.7π Pitch Ratio and 30-Degree Steering Angle

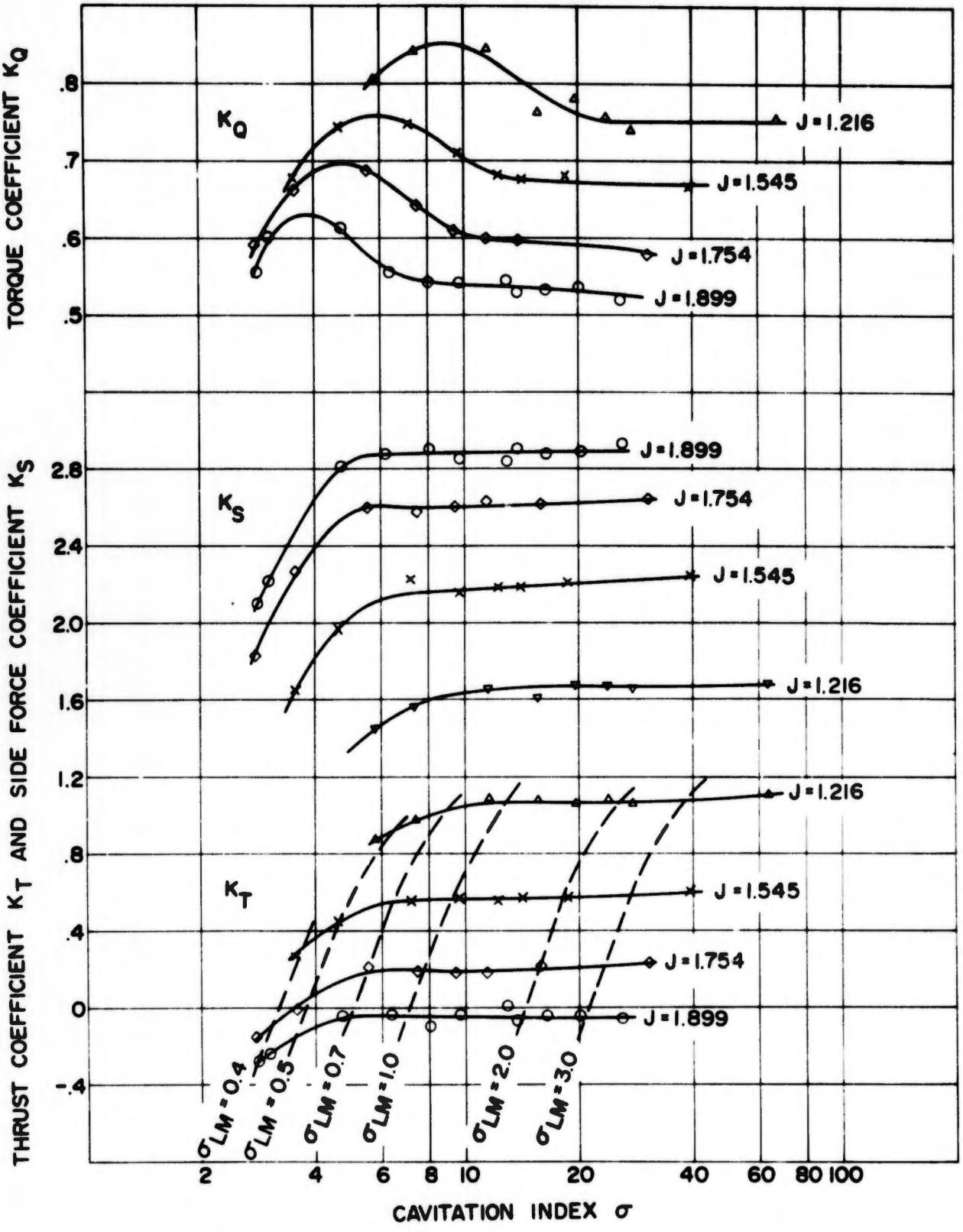

Figure 11 - Propeller Characteristics with Varying Cavitation Number for 0.7π Pitch Ratio and 30-Degree Steering Angle

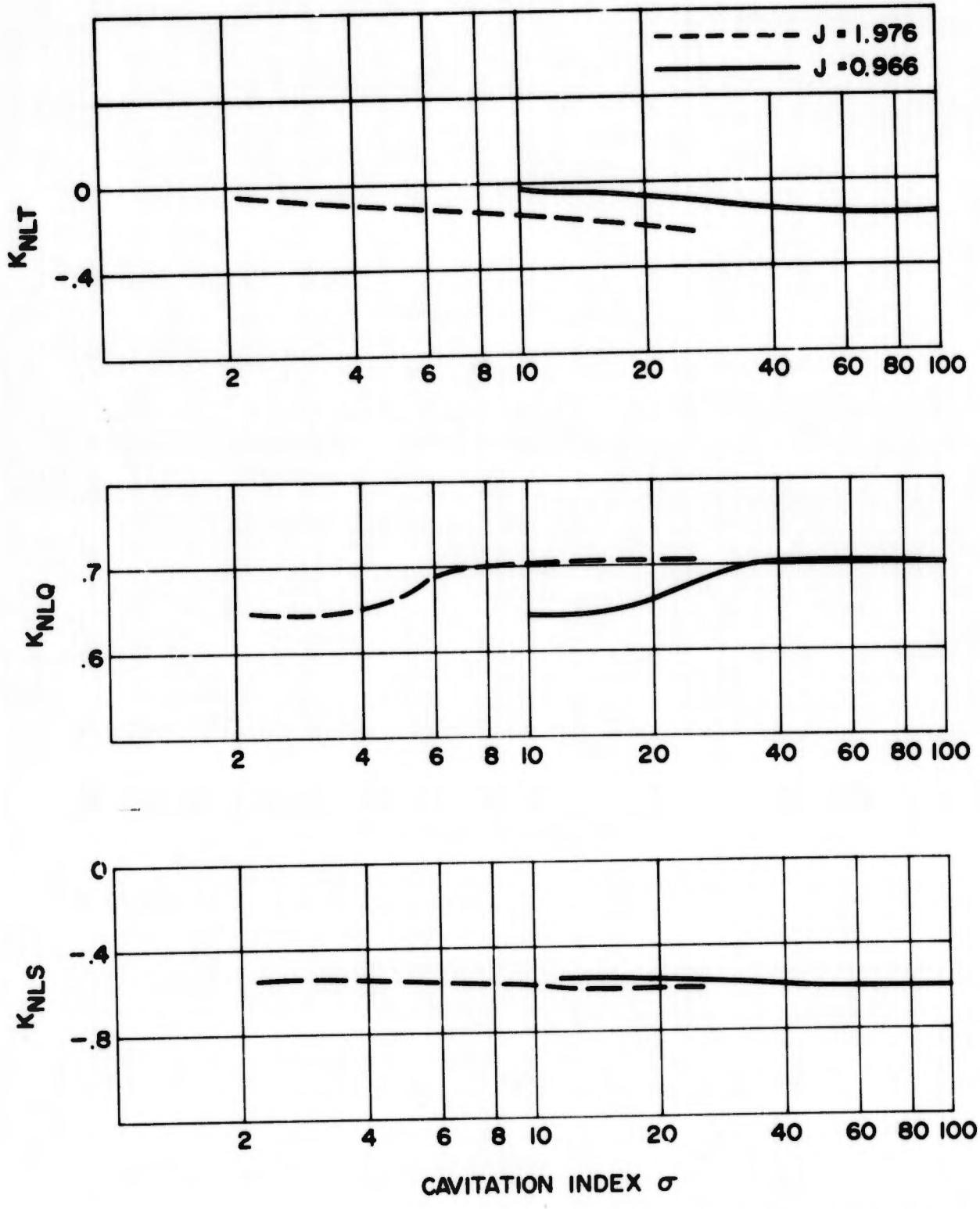

Figure 12 - No-Load Coefficients (0.7π) with Varying Cavitation Number

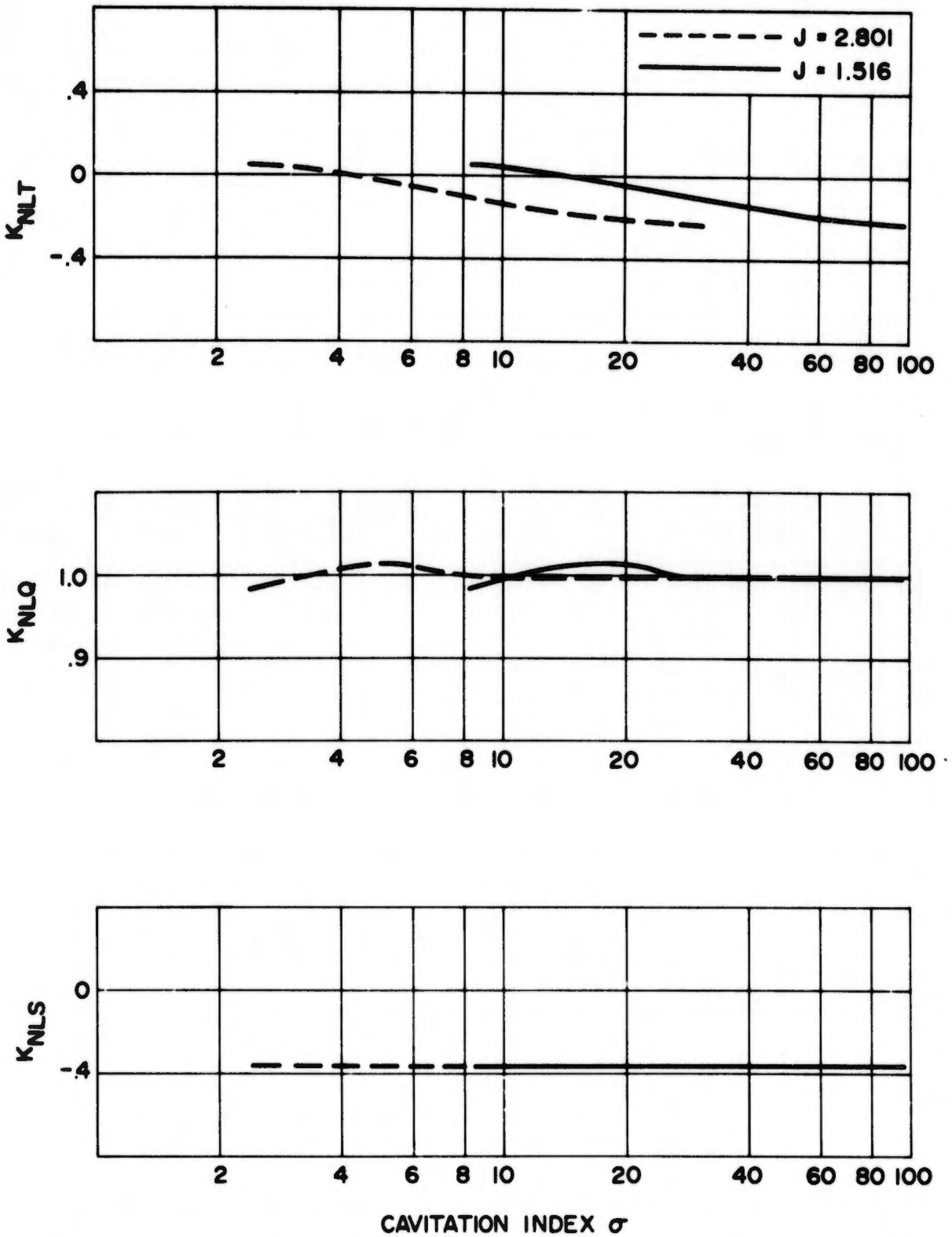

Figure 13 - No-Load Coefficients (0.9_{π}) with Varying Cavitation Number

J = 1.977, σ = 2.46

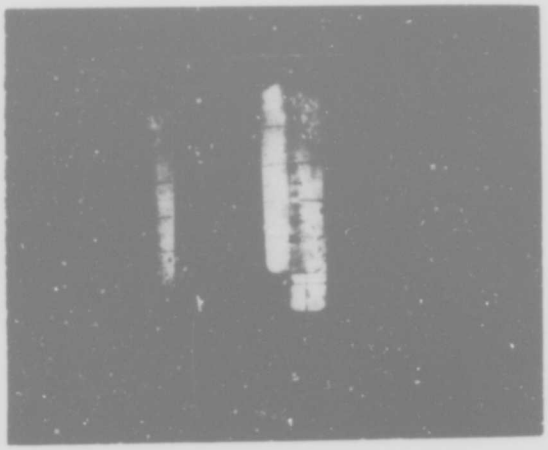

J = 1.668, σ = 3.46

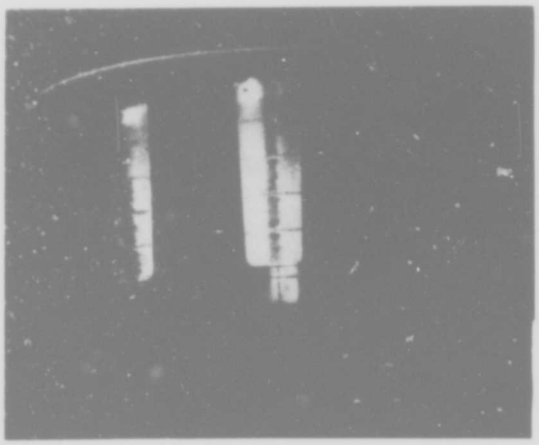

J = 1.352, σ = 8.62

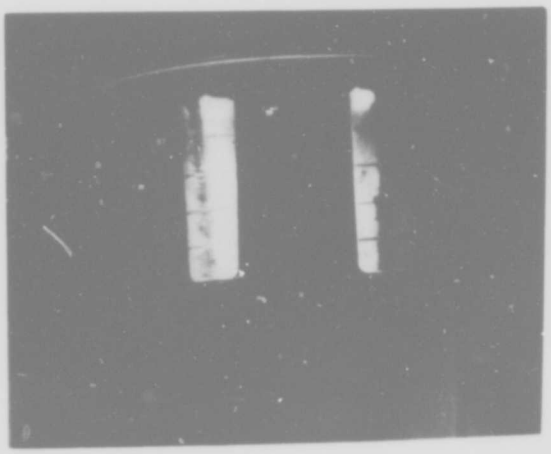

J = 0.966, σ = 25.02

Figure 14 - Photographs of the Propeller at Various Test Conditions
($P/D = 0.7\pi$, $\phi = 0$)

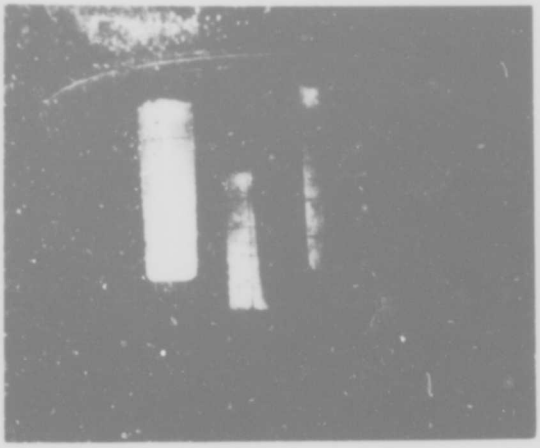

J = 1.899, σ = 13.01

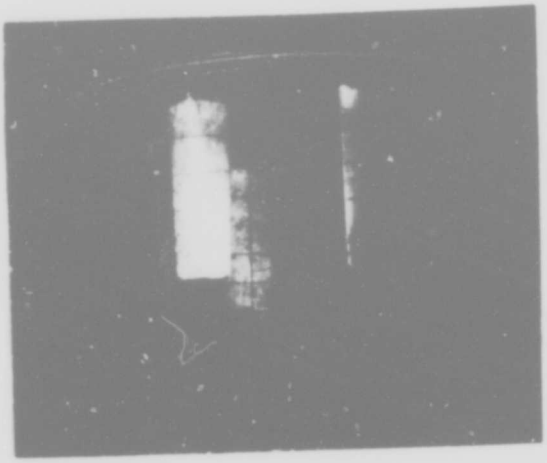

J = 1.754, σ = 9.52

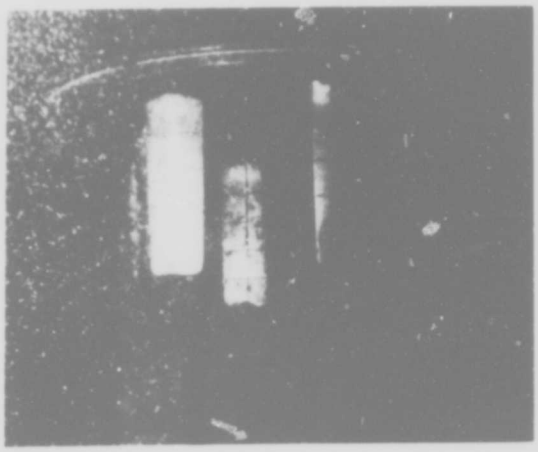

J = 1.545, σ = 9.71

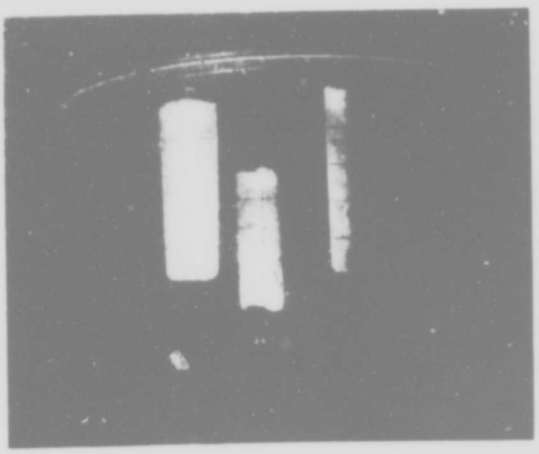

J = 1.216, σ = 15.66

Figure 15 - Photographs of the Propeller at Various Test Conditions
($P/D = 0.7\pi$, $\phi = 30^{o}$)

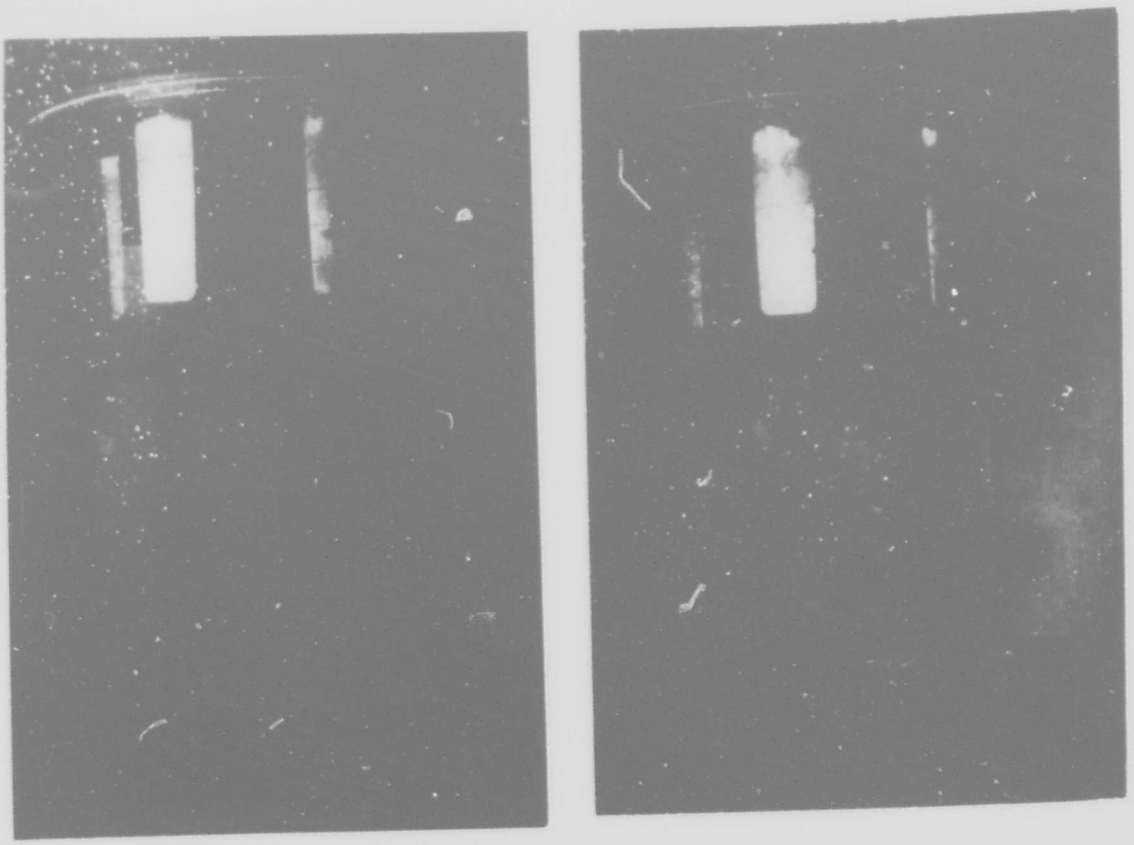

J = 1.802, σ = 5.32

J = 1.516, σ = 8.29

Figure 16 - Photographs of the Propeller at Various Test Conditions
(P/D = 0.9π, ϕ = 0)

Figure 17 - Sketches of Cavitation (P/D = 0.7π, ϕ = 0)

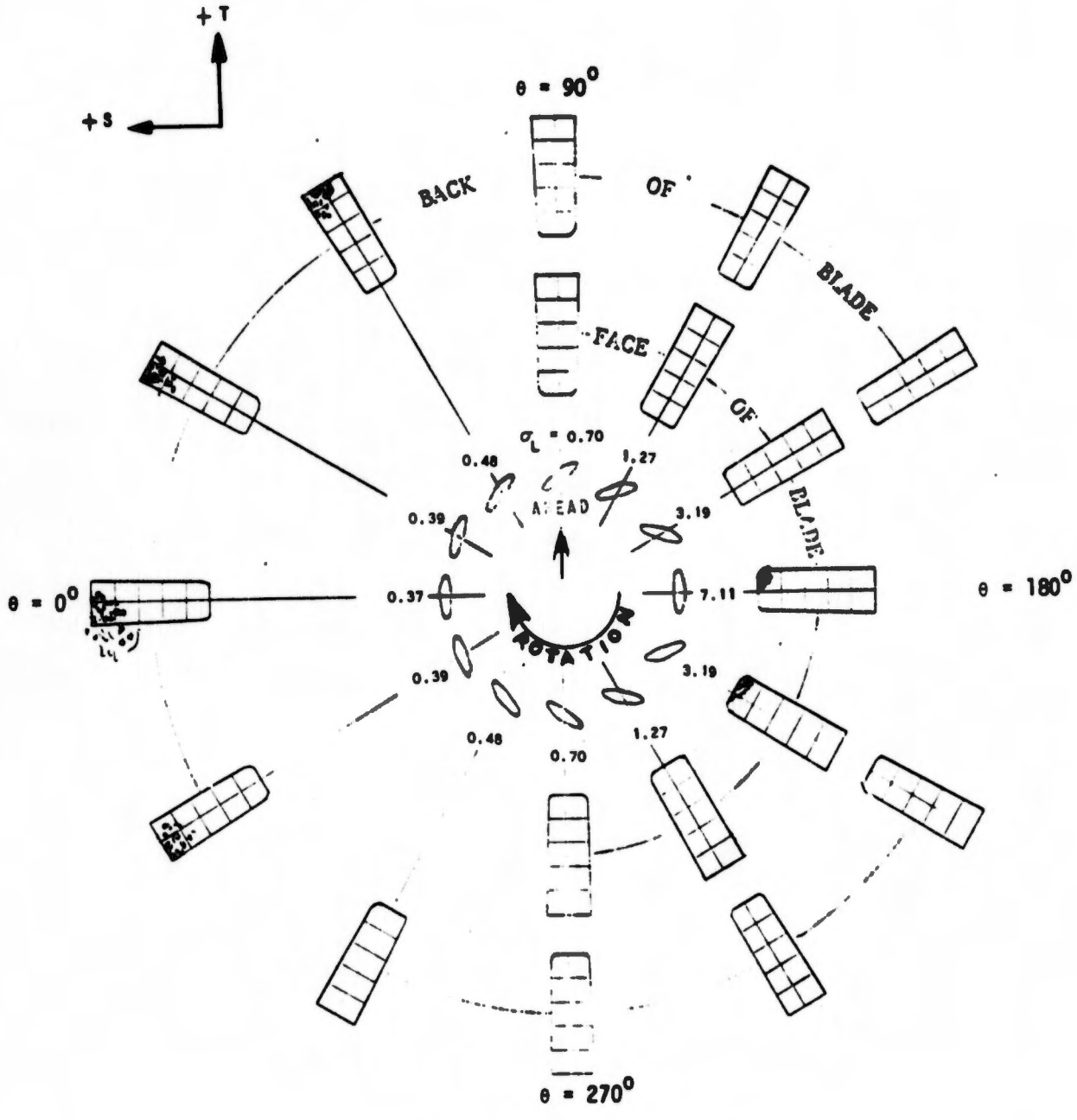

Figure 17a - J = 1.977, σ = 2.46

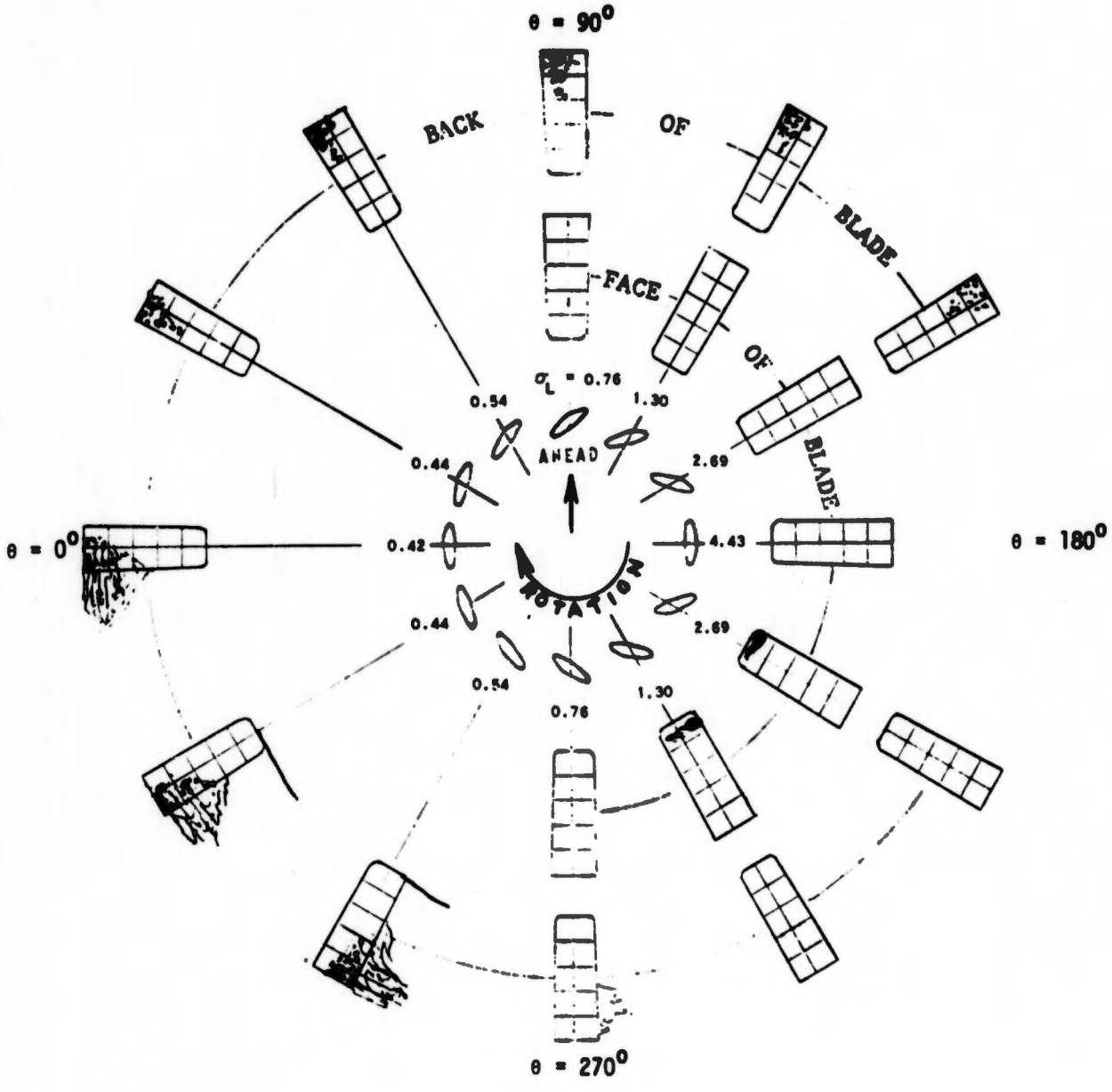

Figure 17b - J = 1.668, σ = 3.46, (P/D = 0.7π, ϕ = 0)

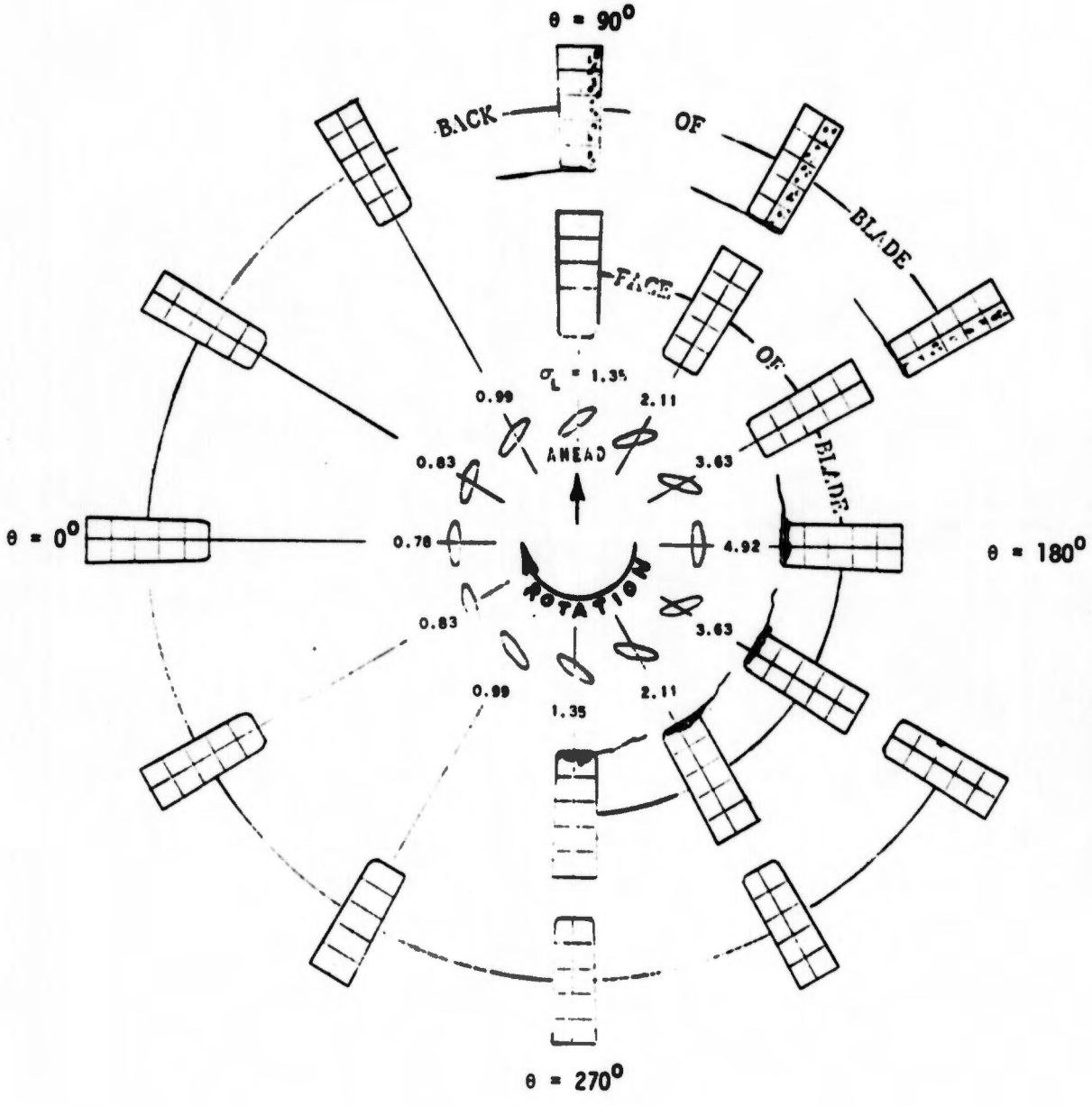

Figure 17c - J = 1.352, σ = 8.62, (P/D = 0.7π, ϕ = 0)

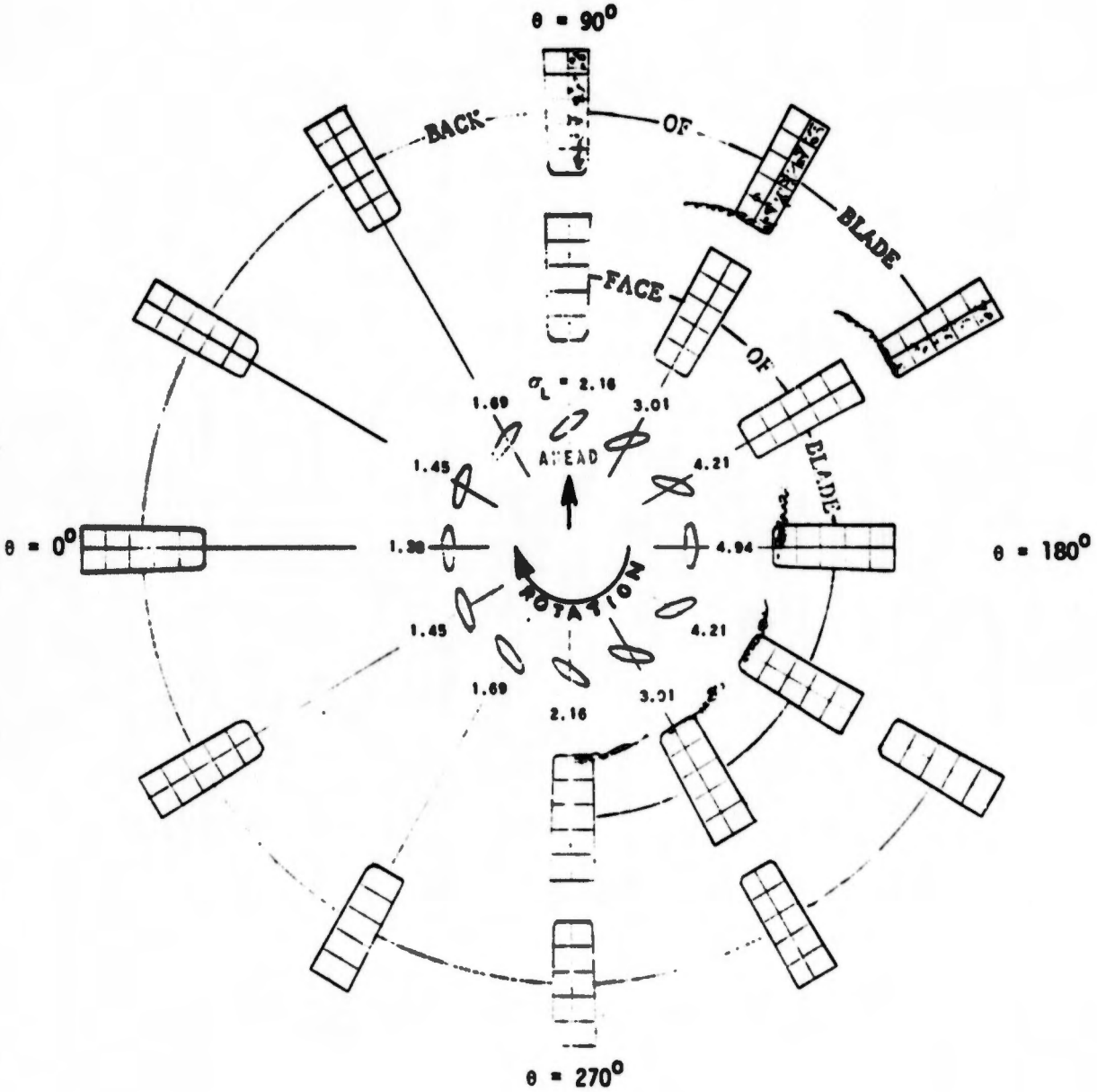

Figure 17d - J = 0.966, σ = 25.02, (P/D = 0.7π, ϕ = 0)

Figure 18 - Sketches of Cavitation (P/D = 0.7π, ♦ 30 Degrees)

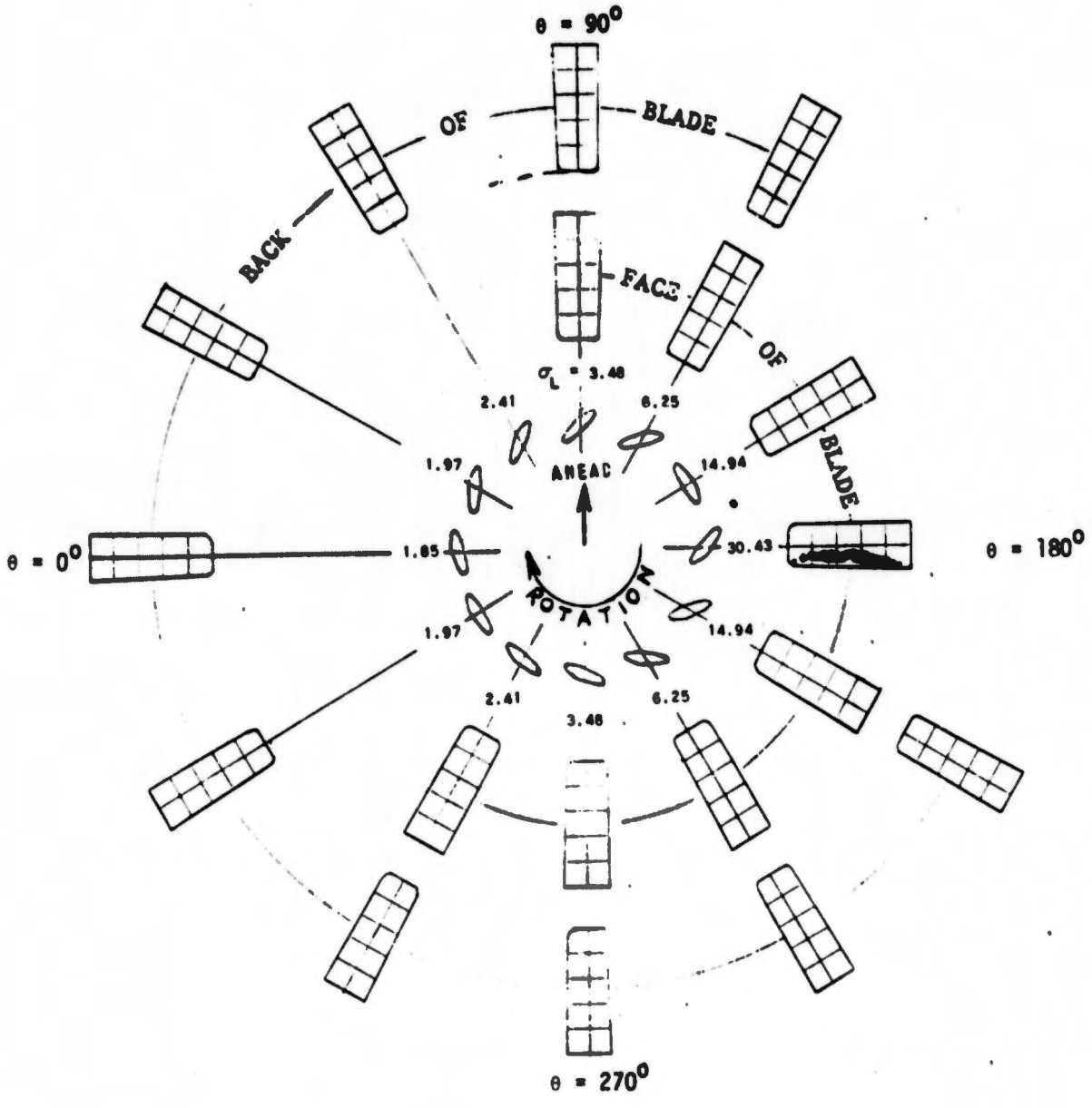

Figure 18a - J = 1.899, σ = 13.01

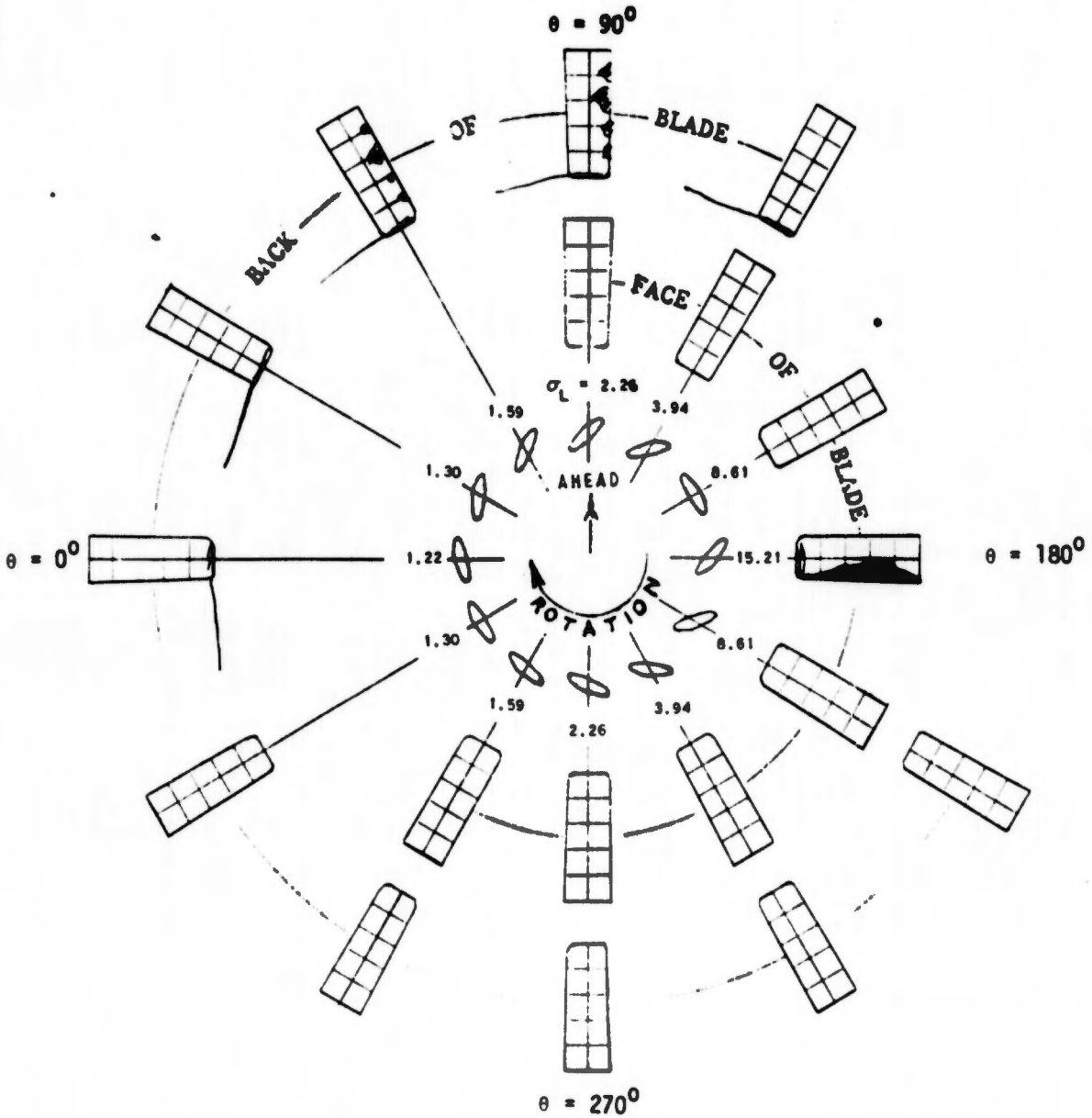

Figure 18b - J = 1.754, σ = 9.52, (P/D = 0.7π, ϕ = 30°)

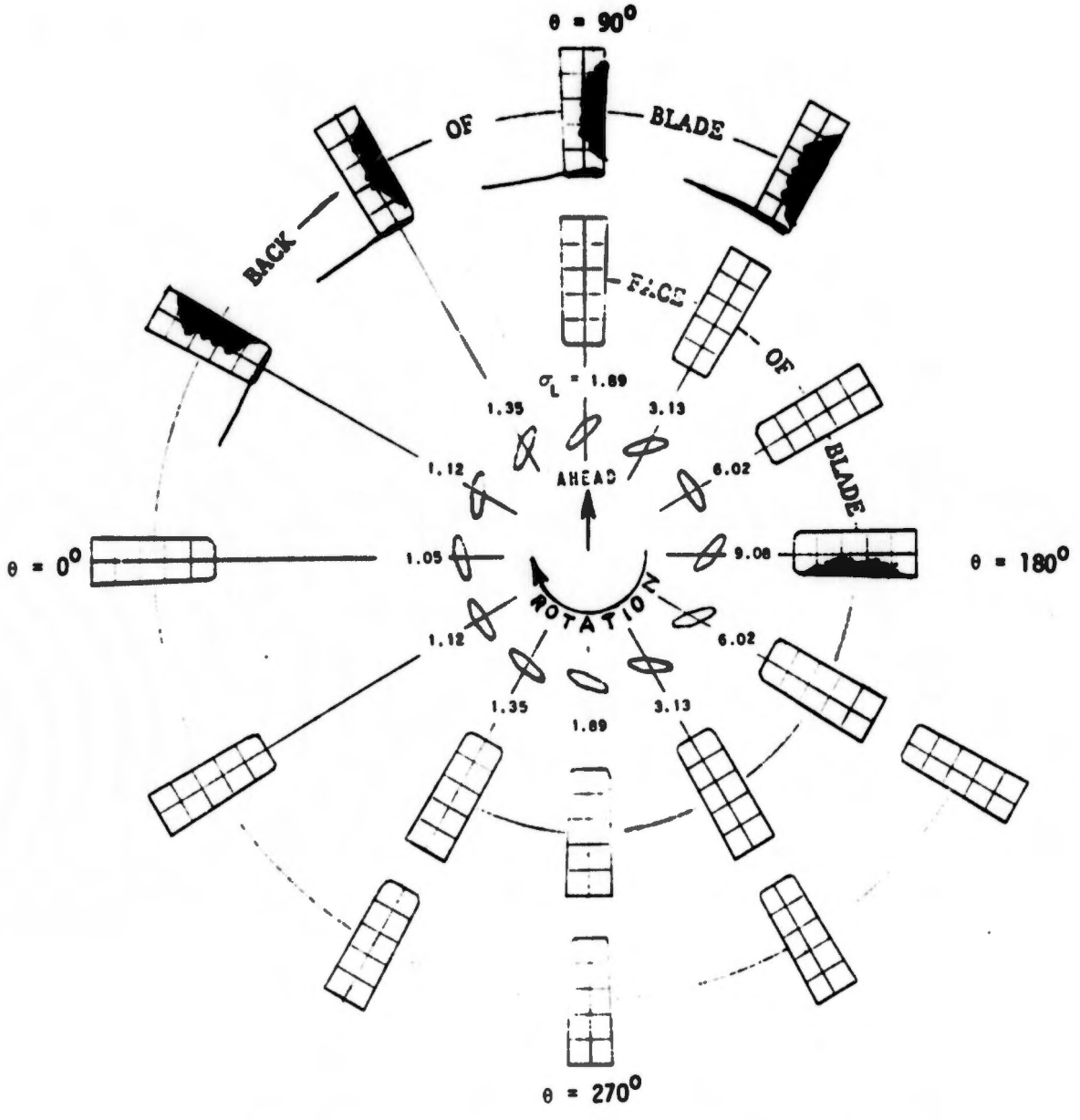

Figure 18c - J = 1.545, σ = 9.71, (P/D = 0.7π, ϕ = 30°)

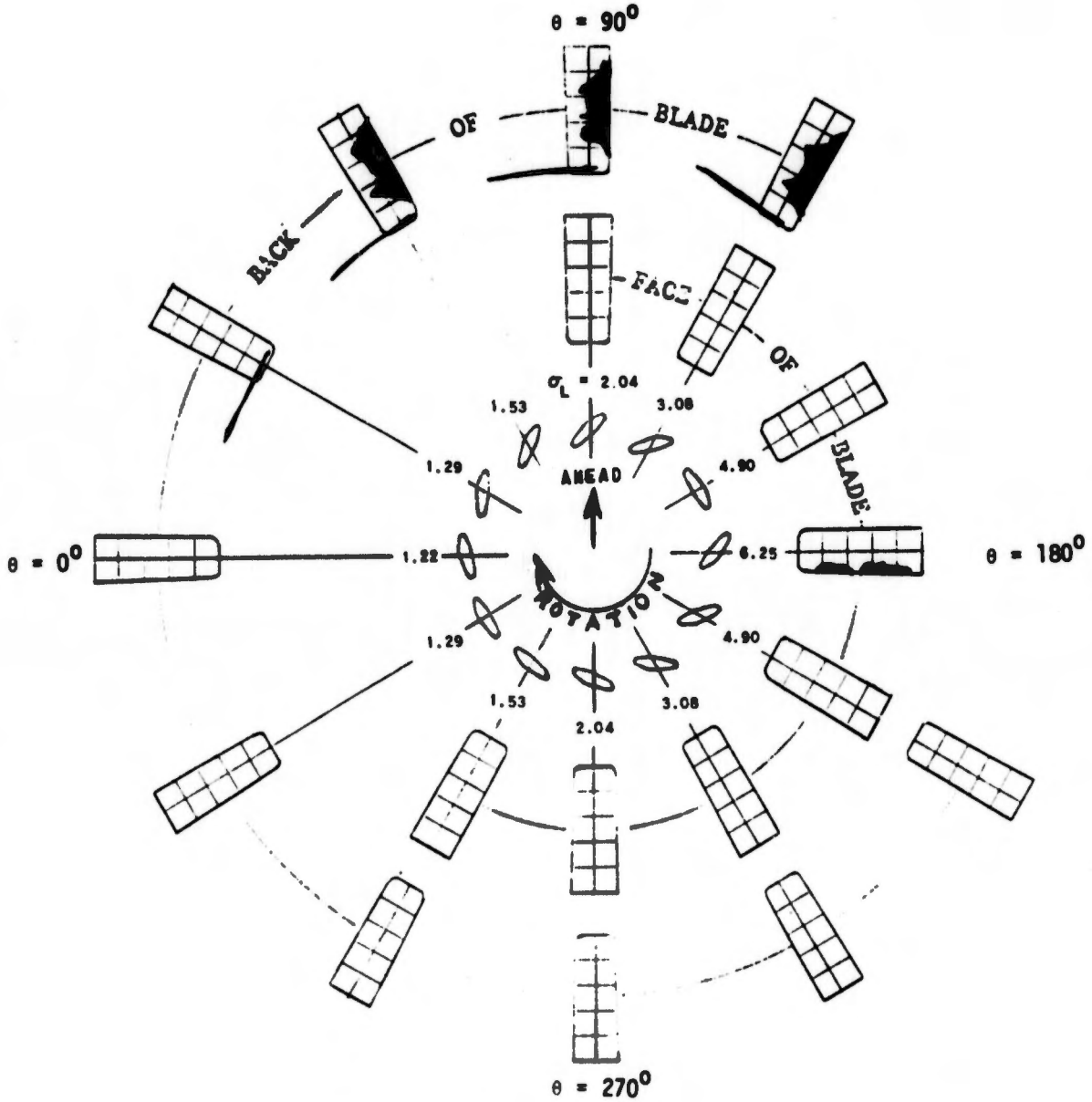

Figure 18d - J = 1.216, σ = 15.66, (P/D = 0.7π, ϕ = 30°)

Figure 19 - Sketches of Cavitation (P/D = 0.9π, ϕ = 0)

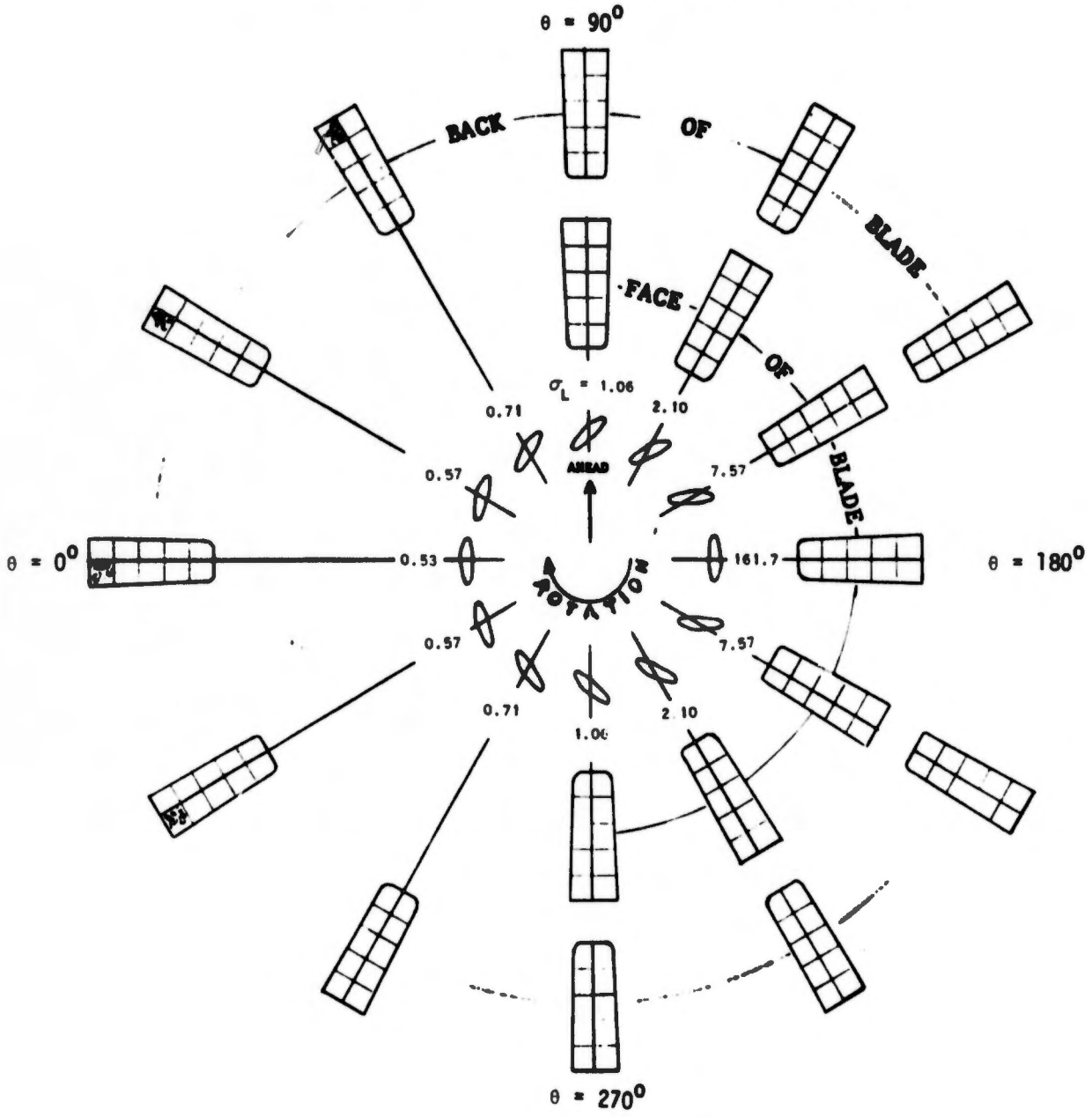

Figure 19a - J = 2.801, σ = 2.39

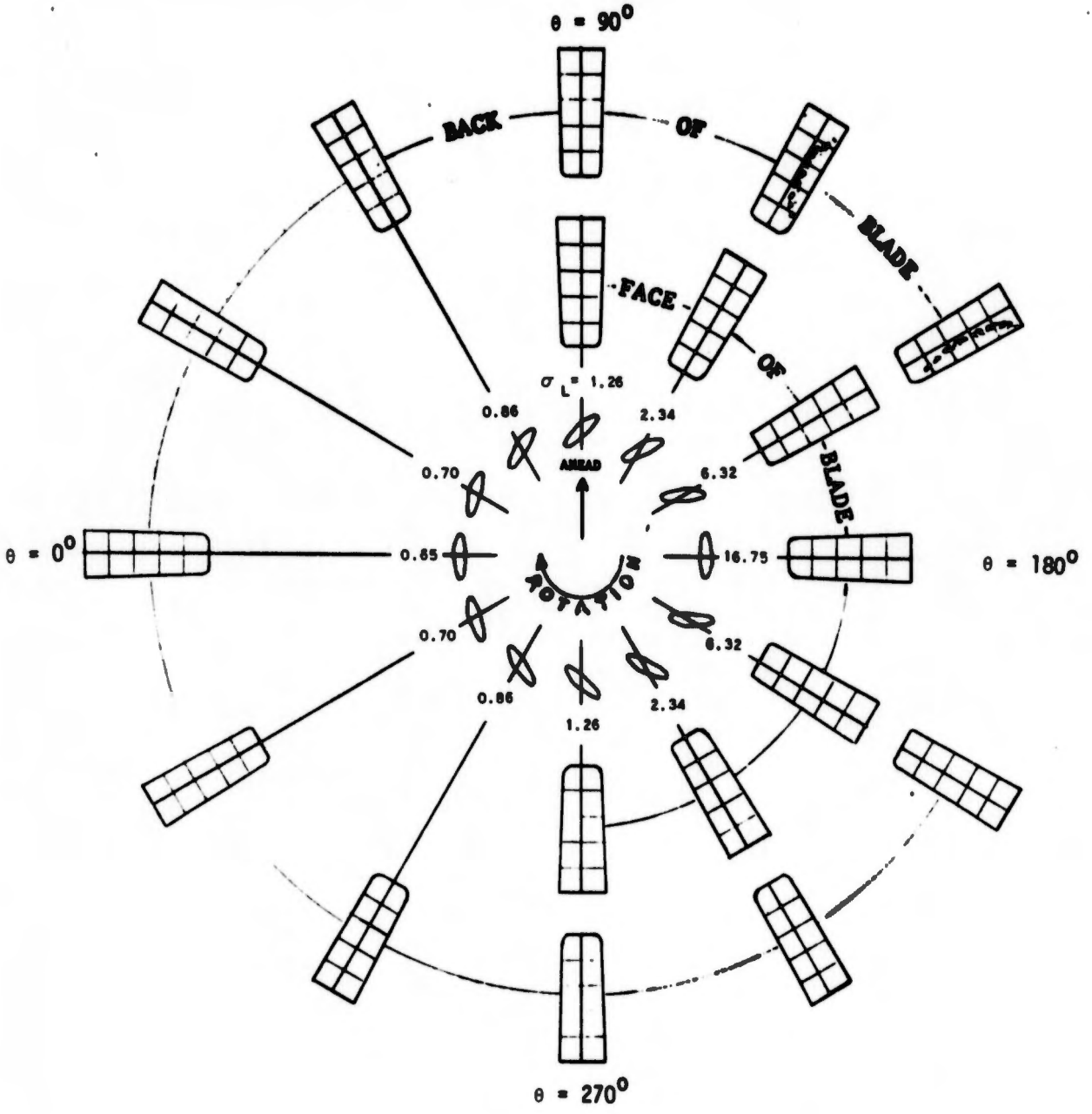

Figure 19b - J = 2.106, σ = 4.05, (P/D = 0.9π, ϕ = 0)

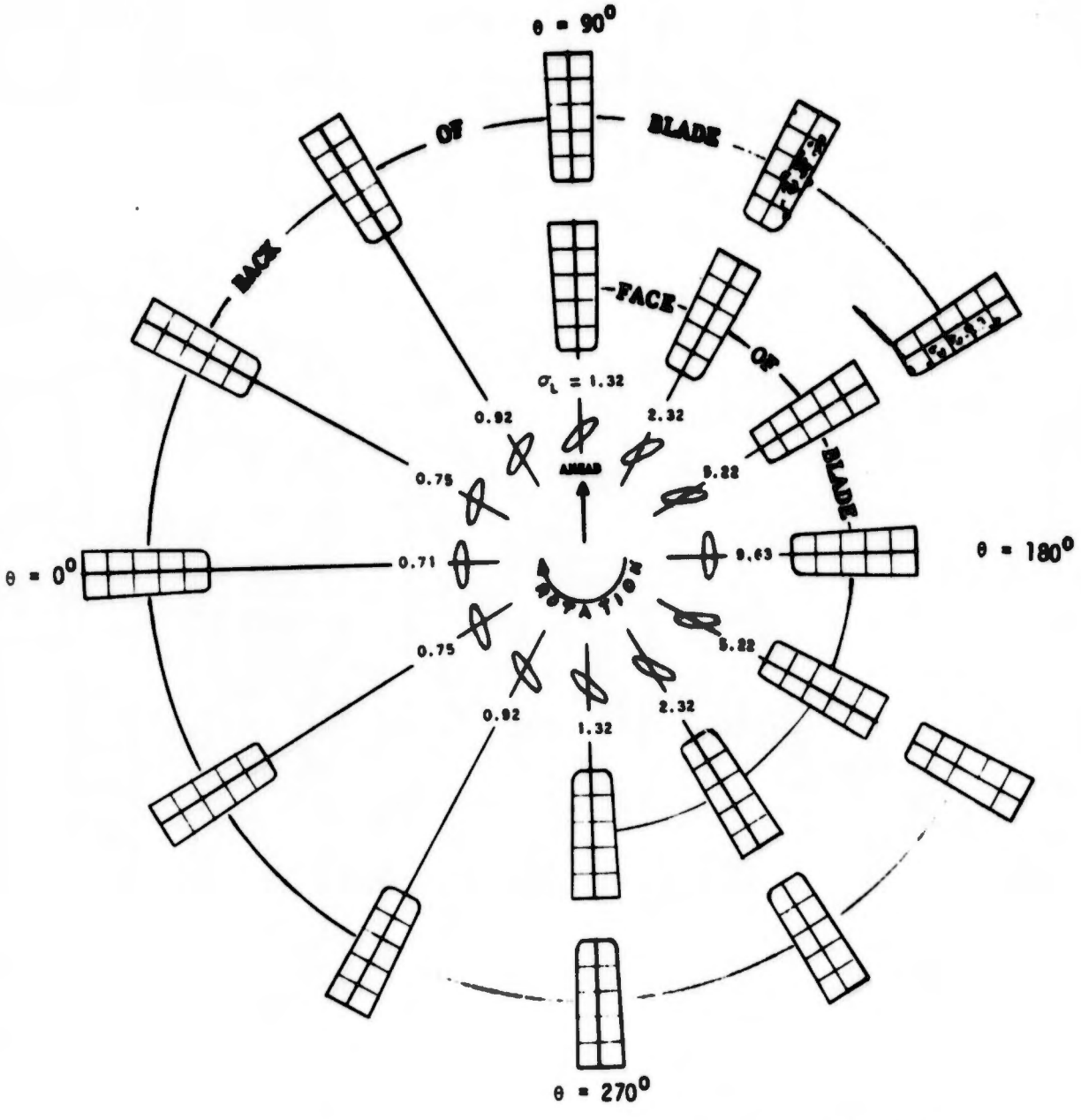

Figure 19c - J = 1.802, σ = 5.32, (P/D = 0.9π, ϕ = 0)

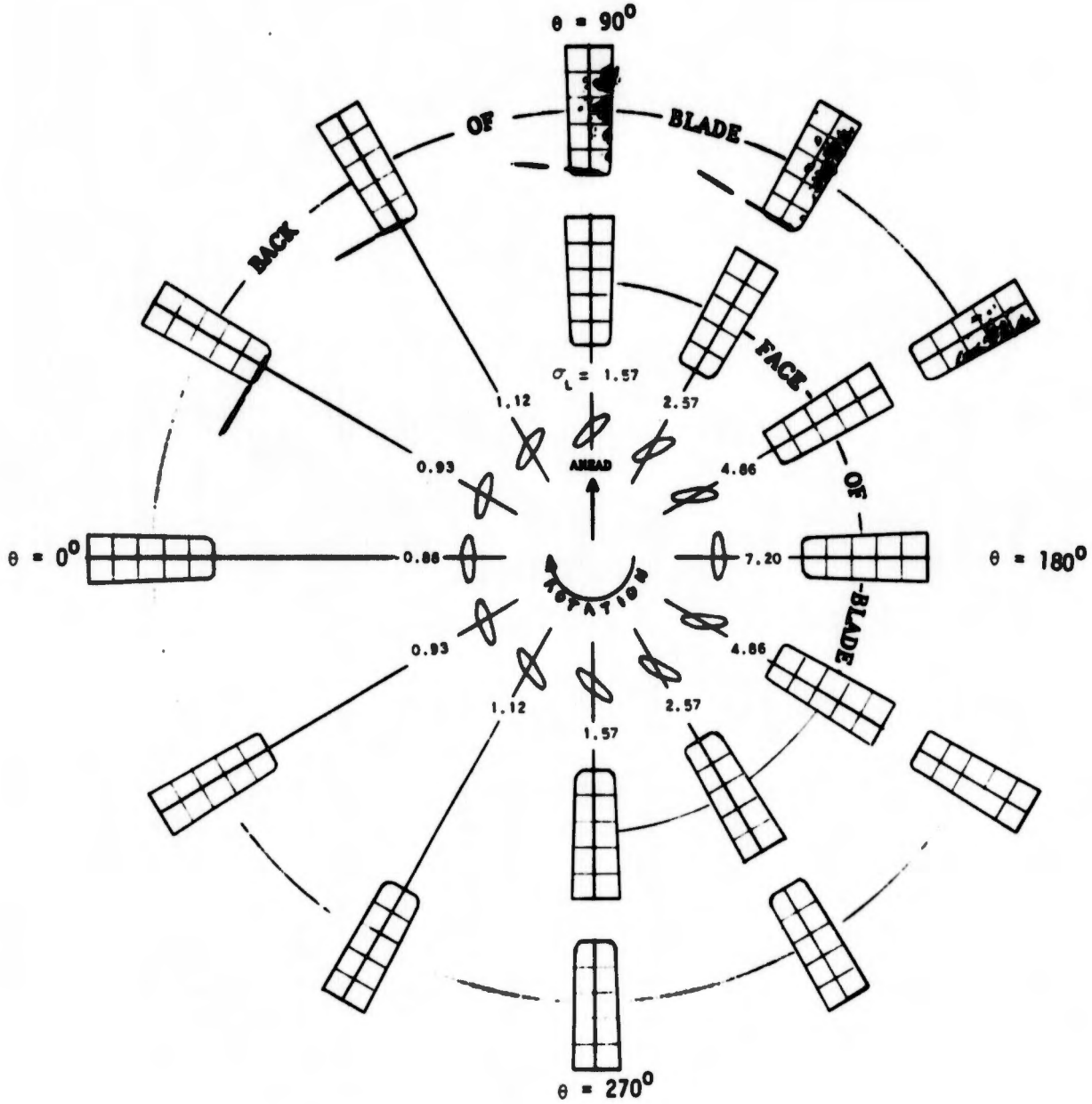

Figure 19d - J = 1.516, σ = 8.29, (P/D = 0.9π, ϕ = 0)

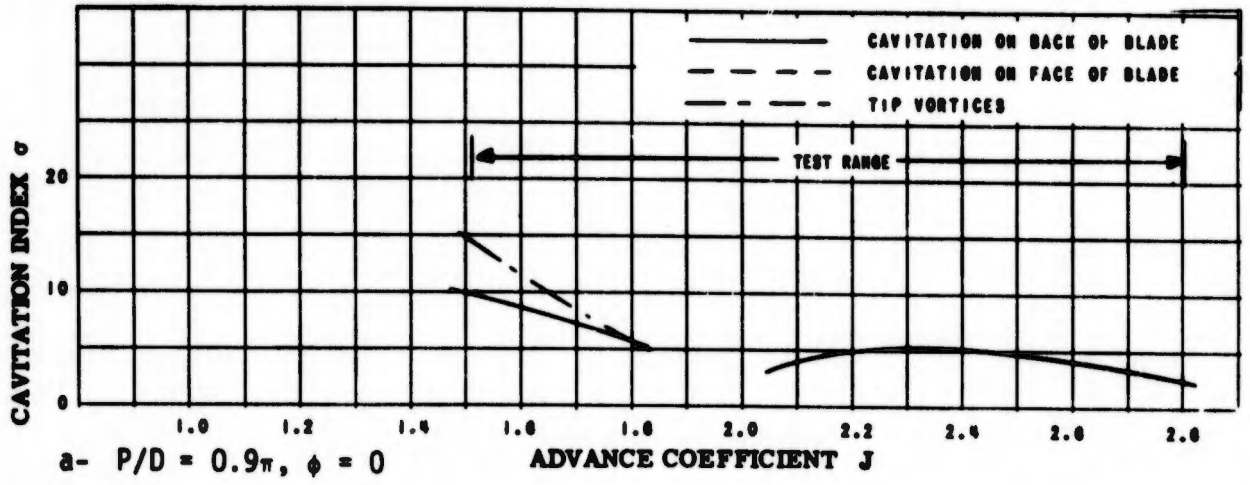

a- P/D = 0.9π, ϕ = 0

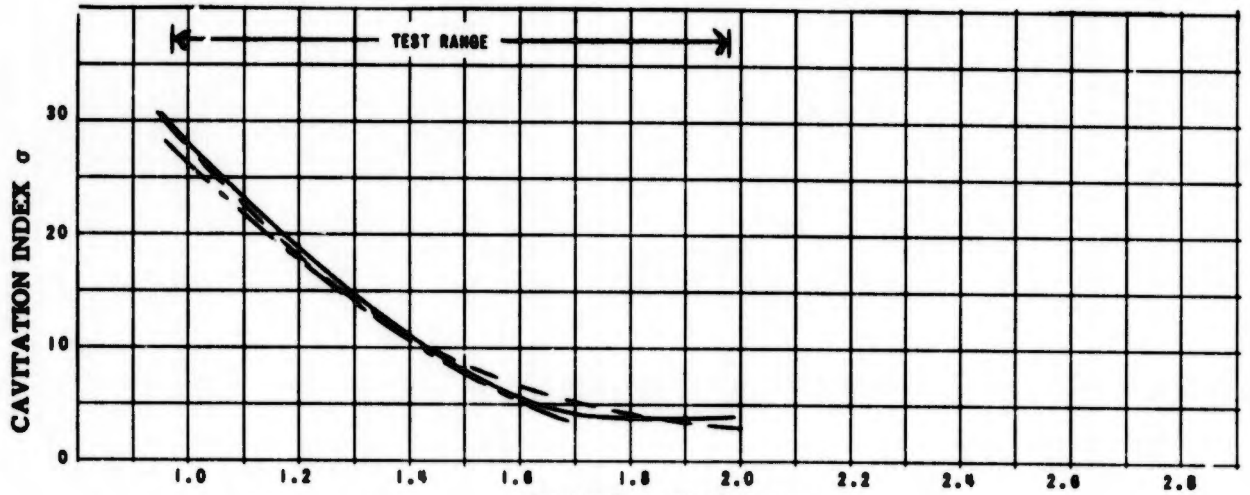

b- P/D = 0.7π, ϕ = 0

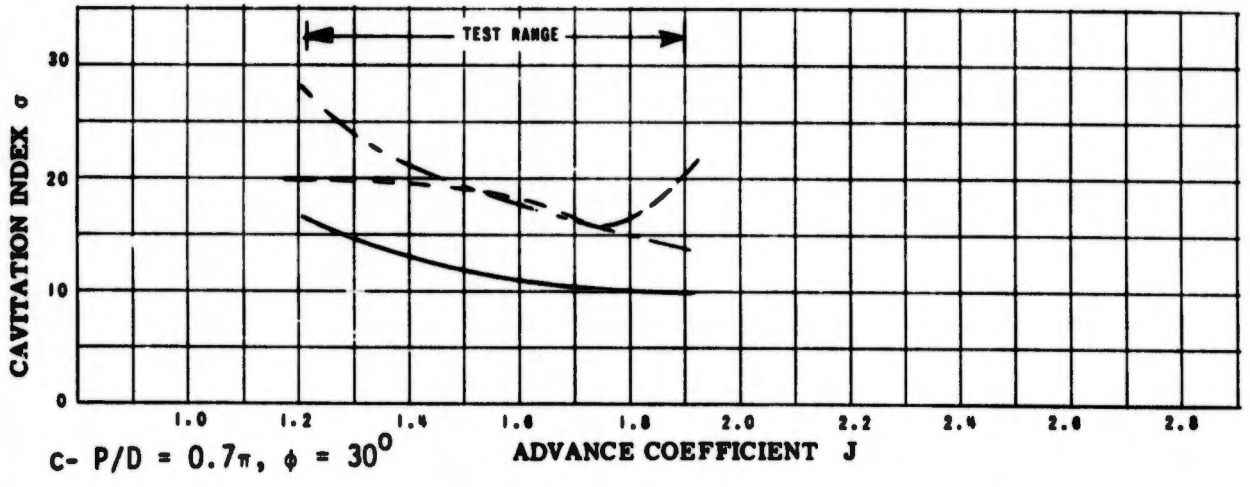

c- P/D = 0.7π, ϕ = 30°

Figure 20 - Inception of Visible Cavitation with Varying Advance Coefficients